Insights into carbonate environmental conditions in the Chukchi Sea

Claudine Hauri[1], Brita Irving[1], Sam Dupont[2,3], Rémi Pagés[1], Donna D. W. Hauser[1], and Seth L. Danielson[4]

[1] International Arctic Research Center, University of Alaska Fairbanks, Fairbanks, AK 99775, USA

[2] Department of Biological and Environmental Sciences, University of Gothenburg, Fiskebäckskil 45178, Sweden

[3] Radioecology Laboratory International Atomic Energy Agency (IAEA), Marine Laboratories, Principality of Monaco

[4] College of Fisheries and Ocean Science, University of Alaska Fairbanks, Fairbanks, AK 99775, USA

Correspondence email: chauri@alaska.edu

Abstract

Healthy Arctic marine ecosystems are essential to the food security and sovereignty, culture, and wellbeing of Indigenous Peoples in the Arctic. At the same time, Arctic marine ecosystems are highly susceptible to impacts of climate change and ocean acidification. While increasing ocean and air temperatures and melting sea ice act as direct stressors on the ecosystem, they also indirectly enhance ocean acidification, accelerating the associated changes in the inorganic carbon system. Yet, much is to be learned about the current state and variability of the inorganic carbon system in remote, high-latitude oceans. Here, we present time-series (2016-2020) of pH and the partial pressure of carbon dioxide (pCO_2) from the northeast Chukchi Sea continental shelf. The Chukchi Ecosystem Observatory includes a suite of subsurface year-round moorings sited amid a biological hotspot that is characterized by high primary productivity and a rich benthic food web that in turn supports coastal Iñupiat, whales, ice seals, walrus (*Odobenus rosmarus*), and Arctic cod (*Boreogadus saida*). Our observations suggest that near-bottom waters (33 m depth, 13 m above the seafloor) are a high carbon dioxide and low pH and aragonite saturation state (Ω_{arag}) environment in summer and fall, when organic material from the highly productive summer remineralizes. During this time, Ω_{arag} can be as low as 0.4. In winter, when the site was covered by sea ice, pH was < 8 and Ω_{arag} remained undersaturated under the sea ice. There were only two short seasonal periods with relatively higher pH and Ω_{arag}, which we term ocean acidification relaxation events. In spring, high primary production from sea ice algae and phytoplankton blooms led to spikes in pH (pH > 8) and aragonite oversaturation. In late fall, strong wind-driven mixing events that delivered low CO_2 surface water to the shelf also led to events with elevated pH and Ω_{arag}. Given the recent observations of high rates of ocean acidification, and sudden and dramatic shift of the physical, biogeochemical, and ecosystem

conditions in the Chukchi Sea, it is possible that the observed extreme conditions at the Chukchi Ecosystem Observatory are deviating from carbonate conditions to which many species are adapted.

1. Introduction

The quickly changing Arctic Ocean has climatic, societal, and geopolitical implications for the peoples of the Arctic and beyond (Huntington et al., 2022). Arctic Indigenous Peoples are at the forefront of this change and their food security, food sovereignty, culture, and ways of life depend on healthy Arctic marine ecosystems (ICC, 2015). The Arctic is warming at a rate that is up to four times that of the rest of the globe (Serreze and Barry, 2011; Serreze and Francis, 2006; Rantanen et al., 2022). This phenomenon, called Arctic Amplification, is observed in air and sea temperatures, has accelerated in recent years, and is expected to continue in the future (Rantanen et al., 2022; Shu et al., 2022). Warming exerts a toll on sea ice extent, ice thickness, and the duration of seasonal sea ice cover: ice is forming later in fall and retreating earlier in spring, thereby increasing the length of the open water period (Stroeve et al., 2011; Serreze et al., 2016; Wood et al., 2015; Stroeve et al., 2014). The lowest Arctic wide minimum sea ice extents were recorded during the last 16 years of the 44 year-long satellite time-series (National Snow and Ice Data Center, DiGirolamo et al. (2022)).

At the same time, the Arctic Ocean is vulnerable to ocean acidification. Although oceanic uptake of anthropogenic carbon dioxide (CO_2) increases oceanic CO_2 and decreases pH and calcium carbonate ($CaCO_3$) saturation states of calcite (Ω_{calc}) and aragonite (Ω_{arag}) globally, climate induced changes to riverine input, temperature, sea ice, and circulation are accelerating the rate of ocean acidification in the Arctic Ocean like nowhere else in the world (Woosley and

Millero, 2020; Qi et al., 2022a; Yamamoto-Kawai et al., 2009; Orr et al., 2022; Semiletov et al., 2016; Qi et al., 2017). Recent observational studies propose that freshening of the Arctic Ocean due to increased riverine input may play an even greater role in acidifying the Arctic Ocean than the uptake of anthropogenic CO_2 (Woosley and Millero, 2020; Semiletov et al., 2016). In addition, the cold Arctic waters have naturally low concentrations of carbonate ions (CO_3^{2-}) and are therefore closer to aragonite undersaturation ($\Omega_{arag} < 1$) than more temperate waters (Orr, 2011; Sarmiento and Gruber, 2006), which leads to the chemical dissolution of free aragonitic $CaCO_3$ structures (Bednaršek et al., 2021). Because of the naturally low concentrations of CO_3^{2-}, such high latitude waters have a lower capacity to take up anthropogenic CO_2 and buffer these changes (Orr, 2011). As a result, concentrations of hydrogen ions (H^+) increase and pH decreases faster in the Arctic than in the tropics, for example.

In the Pacific Arctic, the Chukchi shelf waters have warmed by 0.45 ^oC $decade^{-1}$ since 1990, triple the rate since the beginning of the data record in 1922 (Danielson et al., 2020). Direct observations of the inorganic carbon dynamics of the Chukchi Sea are mostly limited to June through November because of the region's remoteness and accessibility during sea ice covered months. Summertime profiles across the Chukchi Sea show steep vertical gradients in inorganic carbon chemistry (Bates, 2015; Bates et al., 2009; Pipko et al., 2002; Mathis and Questel, 2013). Surface waters have a low partial pressure of carbon dioxide (pCO_2) as a result of high primary production after sea ice retreat, leading to aragonite supersaturated conditions, with $\Omega_{arag} > 2$ (Bates, 2015; Bates et al., 2009). In areas with sea ice melt or riverine freshwater influence, Ω_{arag} tends to be lower and at times undersaturated (Bates et al., 2009; Yamamoto-Kawai et al., 2009). At the same time, pCO_2 values near the seafloor are around 1000 µatm as a result of organic matter remineralization, leading to summertime aragonite undersaturation (Mathis and Questel,

2013; Pipko et al., 2002; Bates, 2015). Between September and November, continuous measurements from within a few meters of the surface suggest a mosaic of pCO_2 levels between ~ 200 to 600 µatm, likely due to patchy wind-induced mixing entraining high-CO_2 waters from depth into the surface mixed layer (Hauri et al., 2013). Yamamoto-Kawai et al. (2016) used mooring observations of S, T, and apparent oxygen utilization to estimate dissolved inorganic carbon (DIC), total alkalinity (TA), and Ω_{arag} in bottom waters at their mooring site in the Hope Valley in the southwestern Chukchi Sea to give first insights into year round variability of the inorganic carbon system. They found slightly less intense aragonite undersaturation in spring and winter compared to summer, with a net undersaturation duration of 7.5-8.5 months per year.

The Chukchi Ecosystem Observatory (CEO) is situated in a benthic hotspot (Figure 1) where high primary production supports rich and interconnected benthic and pelagic food webs (Grebmeier et al., 2015; Moore and Stabeno, 2015). The benthos is dominated by calcifying bivalves, polychaetes, amphipods, sipunculids, echinoderms and crustaceans (Grebmeier et al., 2015; Blanchard et al., 2013). Benthic foraging bearded seals (*Erignathus barbatus*), walrus (*Odobenus rosmarus divergens*), gray whale (*Eschrichtius robustus*), and seabirds feed on these calcifiers during the open water season (Kuletz et al., 2015; Jay et al., 2012; Moore et al., 2022). The CEO site, located on the southern flank of Hanna Shoal, is a region of reduced stratification (relative to other sides of the shoal) that likely alternately feels the effects of differing flow regimes located to the west and to the east (Fang et al., 2020). Consequently, the site exhibits relatively weaker currents (Tian et al., 2021) and so is conducive to deposition of sinking organic matter that in turn feeds the local benthos (Grebmeier et al., 2015). Prolonged open-water seasons during periods of high solar irradiance, in combination with an influx of new nutrients and wind mixing, are likely enhancing primary and secondary production as well as advection of

zooplankton (Lewis et al., 2020; Arrigo and van Dijken, 2015; Wood et al., 2015). These physical processes in turn fuel keystone consumers such as Arctic cod (*Boreogadus saida*) and upper trophic level ringed seals (*Phoca hispida*), beluga (*Delphinapterus leucas*) and bowhead whales (*Balaena mysticetus*) as well as predatory polar bears (*Ursus arctos*) and Indigenous People who rely on the marine ecosystem for traditional and customary harvesting (Huntington et al., 2020).

Perturbation of the seawater carbonate system associated with ocean acidification and climate change can have significant physiological and ecological consequences for marine species and ecosystems (Doney et al., 2020). All parameters of the carbonate system (pH, pCO_2, Ω_{arag}, concentrations of HCO_3^-, CO_3^{2-}, etc.) have the potential to affect the physiology of marine organisms while a change in the saturation state (Ω) can lead to the dissolution of unprotected or "free" $CaCO_3$ structures. Recent work has highlighted the importance of local adaptation to the present environmental variability as a key factor driving species sensitivity to ocean acidification (Vargas et al., 2017, 2022). As carbonate chemistry conditions vary enormously between regions, marine organisms are naturally exposed to different selective pressures and can evolve different strategies to cope with low pH or Ω, or high pCO_2. For example, the deep-sea mussel *Bathymodiolus brevior* living around vents at 1600 m depths is capable of precipitating calcium carbonate at pH ranging between 5.36 and 7.30 and highly undersaturated waters (Tunnicliffe et al., 2009). The response to changes in the carbonate chemistry is also modulated by other environmental drivers such as temperature or food availability (e.g. Thomsen et al., 2013; Breitberg et al., 2015). Consequently, no absolute or single threshold is expected for ocean acidification (e.g., Bednaršek et al., 2021) and a pre-requisite to assessing the impact on any biota is the monitoring at a short temporal scale to characterize the present environmental niche.

When it comes to future impacts, the more intense and faster the changes associated with ocean acidification, the more adverse associated biological impacts are expected (Vargas et al. 2017, 2022). As a result, it is anticipated that Arctic marine waters that are experiencing widespread and rapid ocean acidification will potentially undergo severe negative ecosystem impacts (AMAP 2018).

Here, we present satellite sea ice coverage data and four years of nearly continuous salinity, temperature, and pCO_2 data, accompanied by pH, nitrate (NO_3), dissolved oxygen (O_2), and chlorophyll fluorescence data for some of the time (Table 1, Figures 2 and 3). We developed an empirical equation for estimating pH from moored pCO_2, temperature, and salinity and evaluated it using discrete samples collected across the Chukchi Sea, Bering Sea, and Beaufort Sea. Our timeseries allow us to assess the seasonal and interannual variability and controls of the inorganic carbon system in the Chukchi Sea between 2016 and 2020 and characterize the chemical conditions experienced by organisms. We discuss our observations in terms of progressing acidification and implications to organisms in the Chukchi Sea region.

2. Materials and Methods

2.1 The Chukchi Ecosystem Observatory (CEO)

The Chukchi Sea is a shallow shelf sea with maximum depths < 50 m. It is largely a unidirectional inflow shelf system with Pacific origin water entering the Chukchi Sea through the Bering Strait and advecting north into the Arctic Ocean (Carmack and Wassmann, 2006). The CEO (71°36' N, 161°30' W, Figure 1, Hauri et al., 2018) is located along the pathway of waters flowing through Bering Strait (Fang et al., 2020) and thence from the west of Hanna Shoal toward Barrow Canyon to the south, although the wind can also drive waters from the east over

154 the observatory site (Fang et al., 2020). From both shipboard and moored acoustic Doppler
155 current profiler records, the south side of Hanna Shoal mean flow is characterized by a weak
156 southward-directed current (Tian et al., 2021).

157 The observatory consists of oceanographic moorings that sample year-round, equipped with a
158 variety of sensors that measure sea ice cover and thickness (Sandy et al., 2022), light, currents,
159 waves, salinity, temperature, concentrations of dissolved oxygen, nitrate, and particulate matter,
160 pH, pCO_2, chlorophyll fluorescence, zooplankton abundance and vertical migration (Lalande et
161 al., 2021, 2020), the presence of Arctic cod and zooplankton (Gonzalez et al., 2021), and the
162 vocalizations of marine mammals. During some years, the observatory included a third mooring,
163 an experimental "freeze-up detection mooring", which transmitted real-time data of conductivity
164 and temperature throughout the water column until sea ice formation. The primary moorings
165 stretch from the seafloor at 46 m to about 33 m depth, designed to avoid collisions with ice keels.
166 Pressure sensors at the top of the moorings show less than ± 1 m of excursion of the moored
167 sensor package from its deployment mean depth in any given year, indicating that mooring blow-
168 over or diving is not the cause of any observed large variability. Description of the CEO and lists
169 of sensors deployed at the site can be found in Danielson et al. (2017) and Hauri et al., (2018).
170 For this study we focus on the inorganic carbon system and its controlling mechanisms.
171

172 **2.2 pCO_2**

173 We used a CONTROS HydroC CO_2 sensor (4H-Jena Engineering GmbH, Kiel, Germany) to
174 measure pCO_2. The Contros HydroC CO_2 sensor was outfitted with a pump (SBE 5M, Sea-Bird
175 Electronics) that flushes ambient seawater against a thin semi permeable membrane, which
176 serves as equilibrator for dissolved CO_2 between the ambient seawater and the headspace of the

sensor. Technical details about the sensor and its performance are described in Fietzek et al. (2014), who estimated sensor accuracy to be better than 1% with postprocessing.

A HydroC CO_2 sensor has been deployed at the CEO site since 2016. In all deployments, except 2016, HydroC CO_2 sensors were post-calibrated. The lack of post-calibration in 2016 is not expected to negatively affect data quality because a battery failure resulted in data returns only over the first 3 months (August through November). Following a zero interval where the gas was pumped through a soda lime cartridge to create a zero-signal reference with respect to CO_2, and subsequent flush interval to allow CO_2 concentrations to return to ambient conditions, measurements were taken in a burst fashion every 12 or 24 hours depending on deployment year (Table 1). Average pCO_2 values are reported as the mean of the measure interval (Table 1) with standard uncertainty (Equation 1) defined following best practices (Orr et al., 2018) and where the random component is the standard deviation of the mean, and the systematic components include sensor accuracy and estimated error of the regression during calibration.

$$u = \sqrt{u_{\text{systematic}}^2 + u_{random}^2} \quad (1)$$

More than 96% of the time, the relative uncertainty of the pCO_2 data met the weather data quality goal, defined as 2.5% by the Global Ocean Acidification Observing Network (GOA-ON, Newton et al., 2015).

HydroC CO_2 data were processed using Jupyter notebook scripts developed by 4H-Jena Engineering GmbH using pre- and post-calibration coefficients interpolated with any change in the zero-signal reference over the deployment (Fietzek et al., 2014). Further processing using in-house MATLAB scripts included removal of outliers, calculation of the average pCO_2, and calculation of uncertainty estimates for each measure interval.

200 **2.3 pH**

201 A SeapHOx sensor (Satlantic SeaFET™ V1 pH sensor integrated with Sea-Bird Electronics
202 SBE 37-SMP-ODO) was used to concurrently measure pH, salinity, temperature, pressure, and
203 oxygen (Martz et al., 2010). A SeapHOx was deployed at CEO in 2016, 2017, and 2018. No
204 SeapHOx was deployed in 2019 or 2020 due to supply chain delays and communication issues at
205 sea. Unfortunately, measured pH (pH_{SeaFET}) from the 2016 and 2018 SeapHOx deployments
206 were unusable due to high levels of noise in both the internal and external electrodes. In short,
207 we only have usable pH data between August 2017 and August 2018.

208 pH_{SeaFET} data were excluded during a 14-day conditioning period following deployment and
209 were processed with post-calibration corrected temperature and salinity from the SBE37
210 following Bresnahan et al. (2014) using voltage from the external electrode (V_{ext}), and pH_{Vext}
211 (pH calculated from the external electrode of the SeaFET) from an extended period of low
212 variability (18 February 2018). Despite the availability of discrete data from one calibration cast
213 (Cross et al., 2020b; Table 2), pH_{Vex} was used as the single calibration point (Bresnahan et al.,
214 2014) for a variety of reasons: 1) high variability of pH_{SeaFET} (0.0581 pH units) straddling a 12
215 hour window around the discrete sample collection time, 2) high temporal and spatial variability
216 often seen in the Chukchi Sea, and 3) the discrete pH sample was within the published SeaFET
217 accuracy of 0.05 (Table 2, Figure S1). pH_{SeaFET} values are reported as the mean of the measure
218 interval (Table 1) and standard uncertainty is calculated with Equation 1 with the standard
219 deviation of the average (random), and the SeaFET accuracy (systematic). Data handling and
220 processing were done using in-house MATLAB scripts. pH is reported in total scale and at *in*
221 *situ* temperature and depth for the entirety of this paper.
222

2.4 Nitrate

NO_3 measurements were from a Submersible Ultraviolet Nitrate Analyzer (SUNA) V2 by Sea-Bird Scientific. The SUNA is an *in situ* ultraviolet spectrophotometer designed to measure the concentration of nitrate ions in water. SUNA V2 data were processed using a publicly available toolbox (Hennon et al., 2022; Irving, 2021) with QA/QC steps that included thermal and salinity corrections (Sakamoto et al., 2009), assessment of spectra and outlier removal based on spectral counts (Mordy et al., 2020), and concentration adjustments (absolute offset and linear drift) based on pre-deployment and post-recovery reference measurements of zero concentration (DI) water and a nitrate standard and, when available, nutrient samples taken from Niskin bottles near the mooring site (e.g. Daniel et al., 2020).

2.5 CTD and Oxygen

Two CTDs were deployed on the CEO mooring near the HydroC CO_2 depth. The main pumped Sea-Bird SeaCAT (SBE16) has been deployed on the CEO mooring around 33 m depth since 2014. A pumped SBE43 oxygen sensor was deployed with the SBE16 during the 2015-2016, 2017-2018, and 2019-2020 deployments but only data returns from the 2017-2018 deployment is discussed briefly in this manuscript (Figure S2).

The other pumped CTD was a Sea-Bird MicroCAT (SBE37-SMP-ODO), which was integrated with an optical dissolved oxygen sensor (SBE63; Figure S2), and the SeaFET pH sensor within the SeapHOx instrument. The SeapHOx was deployed in fall 2016, 2017, and 2018. The SBE37-SMP-ODO did not record any CTD or oxygen data during the 2016 deployment and only recorded CTD and oxygen data between August and November 3 in 2018 due to battery failure.

246 Processing of these data included temperature and conductivity correction using pre- and
247 post-calibration data following Sea-Bird Application Note 31 and oxygen correction using pre-
248 and post-calibration data following Sea-Bird Module 28. Oxygen was converted from ml/l to
249 µmol/kg following Bittig et al. (2018). Density and practical salinity were calculated using the
250 TEOS-10 GSW Oceanographic Toolbox (McDougall and Baker, 2011).
251 Differences between the two oxygen sensors (SBE43 and SBE63) of approximately 145 to
252 265 µmol/kg were observed over the 2017-2018 deployment, and both moored sensors had
253 varying offsets compared to nearby casts (Figure S2). Therefore, only relative oxygen values
254 from the freshly calibrated SBE63 are discussed in this paper.
255 The freeze-up detection mooring (Figure 6) consisted of four Sea-Bird SBE 37 inductive
256 modem CTD sensors that transmitted in real time hourly temperature, salinity, and pressure data
257 via the surface float from four subsurface depths (8, 20, 30, and 40 m; Hauri et al., 2018).
258
259 **2.6 Development of empirical relationship to estimate pH**
260 Empirical relationships for estimating water column pH have been developed for regions
261 spanning southern, tropical, temperate and Arctic biomes, using a variety of commonly measured
262 parameters (e.g., pH(S, T, NO_3, O_2, Si) Carter et al 2018; pH(O_2,T,S) Li et al., 2016; pH(θ,O_2)
263 Watanabe et al., 2020; pH(NO_3, T, S, P) and pH(O_2, T, S, P) Williams et al., 2016; pH(O_2, T)
264 Alin et al., 2012; pH(O_2, T) and pH(NO_3, T) Juranek et al., 2009). Given the tight coupling
265 between the concentration of H^+ and concentration of CO_2 solution, an empirical relationship for
266 estimating surface pH from pCO_2 was developed by the National Academies of Sciences,
267 Engineering and Medicine (2017) appendix F. Licker et al. (2019) used this empirical
268 relationship to calculate the global average surface ocean pH and found it represented the

relationship for surface water temperatures spanning 5°C to 45°C. Here, we take a similar approach but extend it to water column pH in our cold region using temperature (T) and salinity (S) as additional proxy parameters (Equation 2).

$$pH^{est} = \alpha_0 + \alpha_1 log\,(pCO_2) + \alpha_2 T + \alpha_3 S \quad (2)$$

Where pH^{est} is the estimated value of water column pH, pCO_2 is from the HydroC, and T and S are from the SBE16, and all α (α_0 = 10.4660, α_1= -0.4088, α_2 = 0.0013, α_3 = -0.0001) terms are model-estimated coefficients determined using MATLAB's multiple linear regression algorithm *regress.m* (Chatterjee and Hadi, 1986). After interpolating pH_{SeaFET} (Figure 4, red dots) to the pCO_2 timestamp, the algorithm was trained over an arbitrarily chosen 180-day period (15/9/2017-14/3/2018, Figure 4, dashed box). An uncertainty of 0.0525 for pH^{est} (Figure 3 and Figure S1, gray shading) was determined with Equation 1, where the RMSE (the uncertainty in the estimation) over the entire pH_{SeaFET} timeseries is the random component and the published accuracy of the SeaFET is the systematic component (since the algorithm was trained with pH_{SeaFET}). The algorithm cross-validation and evaluation are discussed in section 3.1. Unless explicitly defined otherwise, observations of pH refer to pH^{est} for the remainder of this paper.

2.7 Carbonate system calculations

Moored data were collected at different sample intervals (Table 1) and were linearly interpolated to the HydroC CO_2 timestamp to enable further calculations. TA, DIC, and Ω_{arag} (Figure 11 a & b and Figure 3d) were calculated based on measured pCO_2, S, T, and pressure (P) and algorithm-based pH (pH^{est}). Due to a lack of data, nutrient concentrations (Si, PO_4, NH_4, H_2S) were assumed to be negligible in the CO2SYS calculations (e.g. deGrandpre et al., 2019; Vergara-Jara et al., 2019; Islam et al., 2017). pH^{est} was used in lieu of pH_{SeaFET} to allow for

292 calculations over the whole pCO_2 record and due to erroneously large variability of DIC and TA
293 when pH_{SeaFET} was used as an input parameter (Raimondi et al., 2019; Cullison-Gray et al.,
294 2011). The pH-pCO_2 input pair leads to large, calculated errors in DIC and TA (Raimondi et al.,
295 2019; Cullison-Gray et al., 2011) due to strong covariance between the two parameters (both
296 temperature and pressure dependent). Cullison-Gray et al. (2011) attributed unreasonably large
297 short-term variability in calculated TA and DIC to temporal or spatial measurement mismatches
298 between input pH and pCO_2 parameters and found that appropriate filtering alleviated noise
299 spikes. By using pH^{est}, which by the nature of its definition is well correlated to pCO_2, we are
300 eliminating some of these spurious noise spikes. We show Ω_{arag} calculated from pH_{SeaFET}-pCO_2
301 (Figure 3d, red line) because it is less sensitive to calculated errors as it accounts for a small
302 portion of the total CO_2 in seawater (Cullison-Gray et al., 2011).
303 All inorganic carbon parameters were calculated using CO2SYSv3 (Sharp et al., 2023; Lewis
304 and Wallace, 1998) with dissociation constants for carbonic acid of Lueker et al. (2000),
305 bisulfate of Dickson (1990), hydrofluoric acid of Perez and Fraga (1987), and the boron-to-
306 chlorinity ratio of Lee et al. (2010). Sulpis et al. (2020) found that the carbonic acid dissociation
307 constants of Lueker et al. (2000) may underestimate pCO_2 in cold regions (below ~8°C), and
308 therefore overestimate pH and CO_3^{2-}. However, we choose to use Lueker et al. (2000) because
309 they are recommended (Dickson et al., 2007; Woosley, 2021), continue to be the standard (Jiang
310 et al., 2021; Lauvset et al., 2021), and are commonly used at high latitudes (Duke et al., 2021;
311 Raimondi et al., 2019; Woosley et al., 2017). Furthermore, the difference between DIC
312 calculated from pH^{est} and pCO_2 and discrete samples interpolated to moored instrument depth
313 ranged from 266 to -195 µmol/kg using the $K1^*$ and $K2^*$ of Sulpis et al. (2020), compared to -38
314 to -7 µmol/kg using Lueker et al. (2000).

315

316 **2.8 Sea ice concentration**

317 Sea ice concentration at the observatory site was taken from the National Snow and Ice Data
318 Center (NSIDC; DiGirolamo et al., 2022). Latitude and longitude coordinates were converted to
319 NSIDC's EASE grid coordinate system (Brodzik and Knowles, 2002) and the 25-km gridded
320 data were bilinearly interpolated to calculate sea ice concentration at the CEO site. Low sea ice is
321 defined by < 15 % sea ice coverage per grid cell.

322

323 **2.9 Estimation of model-based ocean acidification trend**

324 Model results were obtained from historical simulations of five different global Earth System
325 Models: 1) GFDL-CM4 (Silvers et al., 2018), 2) GFDL-ESM4 (Horowitz et al., 2018), 3) IPSL-
326 CM6A-LR-INCA (Boucher et al., 2020), 4) CNRM-ESM2-1 (Seferian, 2019), and 5) Max Plank
327 Earth System Model 1.2 (MPI-ESM1-2-LR, Wieners et al., 2019) that are part of the Coupled
328 Model Intercomparison Project Phase 6 (CMIP6). Each simulation was used to calculate the
329 annual trend of aragonite saturation state and pH at the closest depth and grid cell to the CEO
330 mooring.

331

332 **3. Results**

333 In the following, we will evaluate the pH algorithm (section 3.1), analyze the large
334 variability patterns (sections 3.2 and 3.3), and then take a closer look at the data from 2020 since
335 the seasonal cycle was different in 2020 than in previous years (section 3.4).

336

337 **3.1 pH algorithm**

The algorithm estimated pH data from the CEO site reasonably well and within the weather uncertainty goal as defined by Newton et al. (2015) most of the time. As a first step, pH^{est} consistency was assessed through cross-validation (Figure 5) using the test dataset (outside the training period, $r^2 = 0.9666$, RMSE = 0.166) and across the whole timeseries ($r^2 = 0.9598$, RMSE = 0.0161, $p<0.0001$, Figure 5). Observed high frequency spikes in pH_{SeaFET} (Figure 4, red dots; Figure 5d, red line) were not captured by the HydroC pCO_2 sensor (sampling frequency of 12 h) and as a result, are not reproduced in the pH^{est} timeseries. Throughout the pH_{SeaFET} timeseries, pH^{est} overestimates pH_{SeaFET} by a mean of 0.0008 and median of 0.0039. Since pH^{est} generally overestimates pH_{SeaFET}, we assume that Ω_{arag} is also somewhat overestimated throughout this manuscript. Discrete water samples were used as reference values to evaluate the algorithm at the CEO site (Table 2) and were found to be within the pH^{est} uncertainty (Figure S1).

An independent verification of our algorithm was done using discrete data collected from the Bering Sea to the Arctic Ocean on four research cruises in 2020, 2019, 2018, and 2017 (Figure 6d; Monacci et al., 2022; Cross et al., 2021; 2020a; 2020b), henceforth called the DBO dataset. Samples collected from deeper than 500 m below the surface or flagged as questionable or bad were excluded from this analysis. pH and pCO_2 were calculated from 1275 discrete samples analyzed for TA, DIC, silicate, phosphate, and ammonium (except when silicate, phosphate, and ammonium were assumed to be negligible for the 327 samples from cruise SKQ202014S; Monacci et al., 2022) using CO2SYSv3 (Sharp et al., 2023; section 2.7 for details) and are referred to as $pH^{disc}{}_{calc}$ and $pCO_2{}^{disc}{}_{calc}$, respectively. $pH^{disc}{}_{est}$ was based on discrete water samples and calculated using Equation 2 and was fit to $pH^{disc}{}_{calc}$ using a linear regression ($r^2 = 0.9975$, RMSE = 0.0078, p-value < 0.0001; Figure 6 a – c). Mean and median differences between $pH^{disc}{}_{calc}$ and $pH^{disc}{}_{est}$ were zero and 0.0022, respectively, with largest anomalies observed at

lower salinities (Figure 6c). Absolute differences between pH^{disc}_{est} and pH^{disc}_{cal} over the salinity range observed at the CEO site (30.87 to 33.93) fall within the weather data quality goal (Newton et al., 2015) 98.7% of the time with maximum absolute differences < 0.03. The uncertainty of 0.0154 for pH^{disc}_{est} was determined using Equation 1, where the mean combined standard uncertainty (u_c) for pH^{disc}_{calc} (0.0133; Orr et al., 2018) was the systmetic component, and the regression RMSE was the random component.

Empirical relationships for estimating water column pH that rely on dissolved oxygen often ignore surface waters to limit biases due to decoupling the stoichiometry of the O_2:CO_2 relationship due to air-sea gas exchange (e.g. Juranek et al., 2011; Alin et al., 2012; Li et al., 2016). We see evidence of this bias in our algorithm at low salinity (Figure 6c) and low pCO_2 (not shown) when compared with the DBO dataset samples collected across the Arctic and from the surface to 500 m, with pH^{disc}_{est} overestimating pH^{disc}_{calc} by a maximum of 0.049. If depth is restricted to between 30 and 500 m when evaluating the algorithm with the DBO dataset, algorithm performance improves ($r^2 = 0.9990$, RMSE = 0.0055, p-value < 0.0001; not shown) and the maximum pH^{disc}_{est} overestimates pH^{disc}_{calc} by 0.022.

3.2 Relaxation events

The sub-surface waters at the CEO site comprise a high pCO_2, low pH, and low Ω_{arag} environment, with mean values of $pCO_2^{mean} = 538 \pm 7$ µatm, $pH^{mean} = 7.91 \pm 0.05$, $\Omega_{arag}^{mean} = 0.94 \pm 0.23$ across the full data record (Figure 3 b - d). In the following we will focus on spikes of high pH and Ω_{arag} and low pCO_2 that occur in spring (May-June) and fall (September-December); we define these spikes as relaxation events (see discussion for justification of term).

383 *Spring:* Springtime relaxation events at 33 m depth that exhibit relatively higher pH and
384 Ω_{arag} and lower pCO_2 compared to the overall mean, are likely consequences of photosynthetic
385 activity during sea ice break-up (Figures 2 and 3). In June of 2018 and 2019, near bottom pH and
386 Ω_{arag} spiked to > 8.17 and > 1.5, respectively, while pCO_2 dropped to < 286 µatm. Ω_{arag} remained
387 oversaturated and pH was greater than 8.0 for nearly all of June in 2018. In 2019, the relaxation
388 event was less sustained, with only four short (2-6 day-long) events of relatively higher pH and
389 $\Omega_{arag} > 1$ in June. In both years, chlorophyll fluorescence spiked and either O_2 increased (in
390 2018) or NO_3 decreased (in 2019), which are signs of photosynthetic activity and primary
391 production.
392 *Fall:* The relaxation events in fall were characterized by large and sudden drops in pCO_2,
393 abrupt increases in pH and Ω_{arag}, and considerable interannual variability in their timing. Unlike
394 the relaxation events observed in spring, we attribute these fall relaxation events to wind-induced
395 physical mixing. To examine the controlling mechanisms causing these abrupt relaxation events
396 in fall, we will start with using water column salinity and temperature data from a freeze-up
397 detection buoy (Hauri et al., 2018) that was deployed in summer 2017 approximately 1 km away
398 from the biogeochemical mooring. The freeze-up detection mooring provided temperature and
399 salinity measurements every 7 meters throughout the water column from the time of its
400 deployment in mid-August until freeze-up. Data from the freeze-up detection mooring suggest
401 that warmer and fresher water from the upper water column gets periodically entrained down to
402 the location of the biogeochemical sensor package at 33 m depth, leading to enhanced variability
403 of density in August and September (Figure 7). Fluctuations of the pycnocline associated with
404 the passage of internal waves could also elevate signal variances. During this time pCO_2 often
405 decreased to or below atmospheric levels and pH sporadically reached values > 8. At the end of

September, a strong mixing event (with coincident strong surface winds) homogenized the water column from the surface down to the location of the sensor package and caused a sudden temperature increase from 0.4 °C to 3.9 °C (Figure 7c and 8a). At the same time, pCO_2 (Figure 7b and 8) decreased from 590 to 308 µatm. This suggests that warm and low CO_2 surface water mixed with CO_2-rich subsurface water and led to a sustained relaxation period that subsequently lasted until mid-November. Another mixing event further eroded the water column stratification and replaced subsurface water with colder and fresher water (ice melt) from the surface at the end of October. This second large mixing event did not lead to large changes in pCO_2, pH, and Ω_{arag}.

Salinity and temperature records from the biogeochemical mooring at 33 m depth also suggest fall season mixing events in all other years, when increases in temperature coincide with decreases in pCO_2 (Figure 2b and c, 3a and 8). For example, two mixing events shaped the carbonate chemistry evolution in fall 2018. pCO_2 decreased from 915 µatm to around 565 µatm and Ω_{arag} increased to 0.9 as temperature increased and salinity decreased in early September (Figures 2 and 8). pCO_2 then increased to 1160 µatm in late October, before decreasing to 385 µatm at the beginning of November, causing a spike in Ω_{arag} to 1.34. At the same time, salinity decreased by 1 unit, suggesting a strong mixing event. Throughout November 2018, pCO_2 oscillated between 344 and 757 µatm and salinity between 31.01 and 32.97, hinting at additional mixing.

Similarly, an early mixing event in 2019 decreased pCO_2 to 352 µatm at the beginning of September. Short-term variability in pCO_2 with maximum levels of up to 855 µatm and minimum values below 300 µatm, variable temperature and salinity, and sporadic aragonite oversaturation events point to mixing through mid-September. At the end of October, a large

mixing event homogenized the water column, accompanied by a decline of salinity by >1 unit, increase of temperature to 4 °C, and decrease of pCO_2 from 565 µatm to below 400 µatm. In a similar fashion to 2018, this fall mixing event was followed by a month-long period of large variability of pCO_2, salinity, pH, and Ω_{arag}, leading to short and sporadic aragonite oversaturation events in November, and sustained oversaturation in December.

3.3 Sustained periods of low pH and Ω_{arag}, and high pCO_2

Waters at 33 m depth at the CEO site were most acidified during the sea ice free periods until mixing events entrained surface waters to the sensor depth (section 3.2). pH and Ω_{arag} started to gradually decrease from their maximum levels (Ω_{arag_max} = 1.65, pH_{max} = 8.19) at the beginning of June in 2018 to their annual low at the beginning of November (Ω_{arag_min} = 0.47, pH_{min} = 7.58, Figure 3 d and c). In November, the waters were also undersaturated with regards to calcite (not shown) and pCO_2 peaked at 1159 µatm (Figure 3b). Dissolved oxygen decreased by about 400 µmol kg^{-1} between July and October, when the sensor stopped working properly. The decrease of dissolved oxygen suggests remineralization of organic material. The decrease of pH, Ω_{arag}, O_2 and increase of pCO_2 was briefly interrupted by a strong mixing event in September, which entrained warmer, fresher, and CO_2-poorer water down to 33 m depth (section 3.2, Figure 8). The 2019 observations paint a similar picture of remineralization during the summer months, as the pCO_2 increase and pH and Ω_{arag} decreases were accompanied by an NO_3 increase (Figure 2d and 3b-d).

pCO_2 steadily increased and pH and Ω_{arag} decreased during the sea ice covered periods (Figures 8). pH was < 8 and Ω_{arag} remained undersaturated under the sea ice. At the same time, NO_3 slowly increased and O_2 decreased, which points to slow organic matter remineralization

(Figure 9). Short-term variability in pCO_2, especially in January of all three observed years, was also reflected in salinity, O_2 and NO_3 (Figure 9) and could be attributed to advection, as the CEO site is adjacent to contrasting regimes of flow and hydrographic properties (Fang et al., 2020).

3.4 Spring and summer of 2020 were different

The seasonal cycle in 2020 strongly contrasted with the previous observed years. pCO_2 gradually increased by roughly 200 µatm throughout the sea ice covered months to 650 µatm when sea ice started to retreat at the beginning of July. By the end of July, pCO_2 doubled and increased to 1389 µatm, which is the highest pCO_2 level recorded in this timeseries. The peak of pCO_2 was accompanied by an increase in salinity of 0.5 while temperature did not change, suggesting the influence of advection. At the beginning of August, pCO_2 dropped to 536 µatm and then oscillated around 600 µatm through much of August before returning to around 900 µatm for the next month. Similarly, pH decreased to 7.5 at the end of July and then oscillated around 7.85, while Ω_{arag} dropped to 0.37, and oscillated around 0.85. The steep drop and oscillation of pCO_2 was reflected in NO_3, suggesting that primary production and remineralization played a role. When pCO_2 and NO_3 decreased at the beginning of August, temperature simultaneously increased by 0.7 °C and salinity decreased by 0.12, suggesting that entrainment of shallower water masses may have played a role too. Comprehensive analyses of the factors that resulted in the 2020 differing conditions are beyond the scope of this paper, but deserve attention in a future effort.

4. Discussion

CEO data provide new insights into the synoptic, seasonal and interannual variability of the inorganic carbon system in a time when ocean acidification and climate change have already started to transform this area. The observations suggest that the CEO site is a high-CO_2 and low-pH and low-Ω_{arag} environment most of the time, except during sea ice break-up when the effects of photosynthetic activity remove CO_2 from the system, and later in fall, when strong storm events entrain low pCO_2 surface waters to the seafloor. Lowest pH and $CaCO_3$ saturation states and highest pCO_2 occur in summer through late fall when organic matter remineralization dominates the carbonate system balance. During this time, Ω_{arag} can fall below 0.5 and even Ω_{calc} becomes sporadically undersaturated ($\Omega_{calc} < 1$).

4.1 pH algorithm

Deploying oceanographic equipment in remote Arctic locations is challenging. The data return from the SeapHOx sensors was disappointingly minimal, despite annual servicing and calibration by the manufacturer. Our new pH algorithm is therefore even more important as it fills pH data gaps in the CEO timeseries and can be applied with confidence from the Bering to the western Beaufort seas (Figure 6). While another successful year of moored pH data return at the CEO site is needed to fully evaluate our algorithm throughout the year, comparison with single discrete water samples nearby the CEO site and the DBO dataset (section 3.1, Table 2, Figures 6 and S1) suggest that our algorithm-derived pH meets the weather quality uncertainty goal of ± 0.02 (Newton et al., 2015) much of the time.

The combination of our new algorithm with recent progress in monitoring pCO_2 with Seagliders (Hayes et al., 2022) will further increase our ability to study the inorganic carbon dynamics at times and locations when shipboard or mooring based measurements may not be

497 practical. Additional assessment is needed to determine to what degree the algorithm needs
498 adjustments beyond the region evaluated in this work.
499
500 **4.2 Uncertainty**
501 Inherent spatial and temporal variability of the inorganic carbon parameters in the
502 Chukchi Sea make the use of discrete water samples for evaluating sensor-based measurements
503 difficult. Historic continuous surface measurements from the area suggest that surface pCO_2 can
504 be as low < 250 µatm in early fall (Hauri et al., 2013), at a time of year when subsurface pCO_2
505 reaches its max of >800 µatm at the CEO site. This suggests a steep pCO_2 gradient of > 17 µatm
506 per meter. High-resolution pH data from the 2017/2018 deployment suggests high temporal
507 variability as well, further complicating the collection of discrete water samples to adequately
508 evaluate the sensors. The HydroC's zeroing function, in addition to our pre- and post-calibration
509 routines that factor into the post-processing of the data, gives us confidence in the accuracy of
510 the pCO_2 data, and further confidence in pH derived from pCO_2.
511 The pH^{est} uncertainty of 0.0525 is likely a conservative estimate based on our validation
512 of pH^{est} (section 3.1, Table 2). Consequently, propagated uncertainties in the calculated
513 parameters are high. As discussed in section 2.7, the pH-pCO_2 input pair exacerbates these larger
514 uncertainties. Mean TA(pH^{est},pCO_2), DIC(pH^{est},pCO_2), and Ω_{arag}(pH^{est},pCO_2), ± u_c (Orr et al.,
515 2018) are 2173 ± 281 µmol kg^{-1}, 2111 ± 263 µmol kg^{-1}, and 0.94 ± 0.23, respectively, when
516 input uncertainties are the standard uncertainty (Equation 1). When the input uncertainty for
517 pH^{est} is only the RMSE of 0.0161 (section 3.1), uncertainties decrease to ± 98 µmol kg^{-1}, ± 93
518 µmol kg^{-1}, and ± 0.09, respectively. When input uncertainties are only the random component of
519 the input parameters (i.e. standard deviation for pH_{SeaFET} and pCO_2 and instrument precision for

520 T and S), TA(pH_{SeaFET},pCO_2), DIC(pH_{SeaFET},pCO_2), and Ω_{arag}(pH_{SeaFET},pCO_2) u_c drops to ± 38
521 μmol kg^{-1}, ± 37 μmol kg^{-1}, and ± 0.06, respectively. Given the above uncertainties and that we
522 do not see significant biofouling at the CEO site, we believe that short term variability can be
523 discussed with confidence with this dataset. In other words, wiggles in the data represent real
524 events, despite the high uncertainty in the precise value of the calculated parameters.
525
526 **4.3 Subsurface biogeochemical drivers of pH, Ω_{arag}, and pCO_2**
527 Inorganic carbon chemistry can be influenced by advection and vertical entrainment of
528 different water masses, temperature, salinity, biogeochemistry, and conservative mixing with TA
529 and DIC freshwater endmembers. Here, we followed Rheuban et al. (2019) and separated the
530 drivers of the observed large pH, Ω_{arag}, and pCO_2 variability to provide additional insights into
531 our timeseries (Figure 10) using CO2SYS by altering input parameters temperature, salinity, TA,
532 and DIC. Anomalies (black) relative to the reference values pH(T_0, S_0, DIC_0, TA_0), Ω_{arag}(T_0, S_0,
533 DIC_0, TA_0), and pCO_2(T_0, S_0, DIC_0, TA_0), were calculated using a linear Taylor series
534 decomposition, adding up the thermodynamic effects of temperature and salinity, and the
535 perturbations due to biogeochemistry, and conservative mixing with freshwater DIC and TA
536 endmembers (Rheuban et al., 2019). Reference values T_0, S_0, DIC_0, and TA_0, are the mean of the
537 CEO timeseries. Freshwater from sea ice melt and meteoric sources (precipitation and rivers)
538 may influence the CEO site. TA and DIC concentrations of 450 μmol kg^{-1} and 400 μmol kg^{-1},
539 respectively, have been measured in Arctic sea ice (Rysgaard et al., 2007). Riverine input along
540 the Gulf of Alaska tends to have lower TA (366 μmol kg^{-1}) and DIC (397 μmol kg^{-1})
541 concentrations (Stackpoole et al., 2016, 2017) than rivers draining into the Bering, Chukchi, and
542 Beaufort Seas (TA = 1860 μmol kg^{-1}, DIC = 2010 μmol kg^{-1}, Holmes et al., 2021) all of which

543 can influence the CEO site to some extent (Asahara et al., 2012; Jung et al., 2021). In this Taylor
544 decomposition we used sea ice TA and DIC endmembers (Rysgaard et al., 2007) but want to
545 emphasize that using Arctic river endmembers did not meaningfully change the results (not
546 shown). Figure 10 shows the effects of biogeochemical processes, temperature, salinity, and
547 conservative mixing with TA and DIC freshwater endmembers on pH, Ω_{arag}, and pCO_2. The
548 effects of salinity (turquoise) and conservative mixing with TA and DIC freshwater endmembers
549 (green) are negligible for pH, Ω_{arag}, and pCO_2. Temperature varied between -1.7 °C during the
550 sea ice covered months and up to 4 °C in late fall, when wind events mixed the whole water
551 column and entrained warm and low pCO_2 surface waters to the instrument depth at 33 m (see
552 section 3.2 for a more in-depth discussion of these mixing events). During this time, the increase
553 in temperature counteracted the effect of biogeochemistry slightly and increased pCO_2 and
554 decreased pH (Figure 10 a,c). Temperature did not affect Ω_{arag}.
555 Biogeochemistry (photosynthesis, respiration, calcification, dissolution) is the most
556 important driver of the inorganic carbon dynamics at 33 m depth at the CEO site. The springtime
557 relaxation events in 2018 and 2019 with relatively higher pH and Ω_{arag}, and lower pCO_2, were
558 mainly driven by biogeochemistry (Figure 10, magenta). During these events O_2 increased and
559 NO_3 decreased, suggesting photosynthetic activity (Figure 2d, e and 3a). Near bottom
560 photosynthetic activity by phytoplankton or sea ice algae has been observed at different locations
561 across the Chukchi Sea (Arrigo et al., 2017; Ouyang et al., 2022; Stabeno et al., 2020; Koch et
562 al., 2020). Sediment trap data from a CEO deployment prior to the start of this pCO_2 and pH
563 time-series suggest that export of the exclusively sympagic sea ice algae *Nitzschia frigida* peaked
564 in May and June, during snow and ice melt events (Lalande et al., 2020), further supporting the
565 hypothesis that sea ice algae contributed to the CO_2 draw down. Interestingly, TA also increased

significantly during these events in 2018 and 2019, which cannot be solely attributed to organic matter production. Specifically, TA increased by 23 umol kg^{-1} in 2019 (Figure 11a). However, with an observed NO_3 decrease of 7.6 umol kg^{-1}, we would expect an increase of TA by 7.6 umol kg^{-1}. This is assuming that NO_3 is the primary source of nitrogen during organic matter formation, and that assimilation of 1 umol of NO_3 leads to an increase of TA of 1 umol (Wolf-Gladrow et al., 2007). The TA increase of 23 umol kg^{-1} is therefore larger than expected from organic matter formation alone and is likely due to $CaCO_3$ mineral dissolution. While direct evidence is missing, the strong TA increase suggests that $CaCO_3$ mineral dissolution during sea ice break up also plays an important role at the CEO site. As observed in other Arctic areas, it is possible that ikaite crystals that were trapped in the ice matrix dissolved in the water column when sea ice melted (Rysgaard et al., 2012, 2007).

4.4 Progression of ocean acidification in the Chukchi Sea

Organisms living at the CEO site may have always been exposed to large seasonal variability and low pH and Ω_{arag} (high pCO_2), but the combined and cumulative effects of climate change and ocean acidification have rapidly made these conditions more extreme and longer lasting. Ocean acidification serves as a gradual environmental press by increasing the system's mean and extreme pCO_2 and decreasing mean and extreme pH and Ω_{arag}. Climate induced changes to other important controls of the inorganic carbon system, such as sea ice, riverine input, temperature, and circulation can act as sudden pulses and further modulate the inorganic carbon system to a less predictable degree and cause extreme events (Woosley and Millero, 2020; Orr et al., 2022; Hauri et al., 2021; Qi et al., 2017). Huntington et al. (2020) describe a sudden and dramatic shift of the physical, biogeochemical and ecosystem conditions

589 in the Chukchi and Northern Bering seas in 2017. For example, satellite data for the CEO site
590 illustrate that the longest open water seasons on record occurred between 2017 and 2020. Before
591 2017, the open water season was on average 81 (± 40) days long (i.e., below 15 %
592 concentration), of which 60 (± 44) days were ice free, whereas between 2017 and 2020, the low
593 sea ice period was 157 (± 30) days long, of which 152 (± 24) days were ice free (Figure 12). Sea
594 ice decline and increased nutrient influx has also promoted increased phytoplankton primary
595 production in the area (Lewis et al., 2020; Arrigo and van Dijken, 2015; Payne et al., 2021).
596 Since our inorganic carbon timeseries started after the "dramatic shift" that was observed in the
597 Chukchi Sea in 2017 (Huntington et al., 2020) and given the uncertainty in model output in this
598 region, we can only speculate about how the changes in sea ice, temperature and biological
599 production may have affected seasonal variability and extremes of the inorganic carbon
600 chemistry at the CEO site. However, since the summertime low pH and Ω_{arag} and high pCO_2 are
601 tightly coupled to the length of the ice-free period and intensity of organic matter production, it
602 is possible that the observed summertime period of extreme conditions may have been
603 previously unexperienced at this site. We therefore think it is justified to call the spikes of pH
604 and Ω_{arag} "ocean acidification relaxation events", since the long-lasting summertime period of
605 extremely low pH and Ω_{arag} may be a new pattern.
606
607 **4.5 Relevance for ecosystem**
608 Marine organisms are exposed to a wide range of naturally fluctuating environmental
609 conditions such as temperature, salinity, carbonate chemistry and food concentrations that
610 together constitute their ecological niche. As evolution works toward adaptation, the tolerance
611 range of species and ecosystems to such parameters varies between locations and is often closely

612 related to niche status (Vargas et al., 2022). Stress can be defined as a condition evoked in an
613 organism by one or more environmental and biological factors that bring the organism near or
614 over the limits of its ecological niche (after Van Straalen, 2003). The consequence of the
615 exposure to a stressor will depend on organismal sensitivity, stress intensity (how much it
616 deviates from present conditions) and stress duration. In a synthesis of the global literature on the
617 biological impacts of ocean acidification, Vargas et al. (2017, 2022) showed that the extreme of
618 the present range of variability of carbonate chemistry is a good predictor of species sensitivity.
619 In other words, larger deviations from present extreme high pCO_2 or extreme low pH, would be
620 expected to exert more negative biological impacts. Organismal stress and niche boundaries have
621 implications for the definition and understanding of controls and future ocean acidification
622 conditions in experiments aimed at evaluating future biological impacts.
623 Our data provide insights on conditions that affect and determine local species'
624 ecological niches, and a necessary key is to evaluate or re-evaluate their sensitivity to present and
625 future carbonate chemistry conditions, particularly for the sessile benthic calcifiers that constitute
626 prey for mobile and upper trophic level taxa. For example, an experimental study on three
627 common Arctic bivalve species (*Macoma calcarean, Astarte montagui* and *Astarte borealis*)
628 collected in the CEO concluded that these species were generally resilient to decreasing pH
629 (Goethel et al., 2017). However, only two pH were compared (a "control" (pH of 8.1) and an
630 "acidified" treatment (pH of 7.8) and our results show that organisms are already experiencing
631 more extreme conditions today than have been experimentally manipulated. While these data
632 provide insights on these species' plasticity to present pH conditions, they cannot be used to infer
633 sensitivity to future ocean acidification or extremes of current conditions. Based on the local
634 adaptation hypothesis (Vargas et al. 2017, 2022), stress and associated negative effect on species

635 fitness can be expected when pH deviates from the extreme of the present range of variability
636 (pH<7.5) as shown in other regions (e.g. echinoderms: Dorey et al., (2013); crustaceans: Thor
637 and Dupont, (2015); bivalves: Ventura et al., (2016)).
638 At the CEO, our results show sustained periods of remarkably low pH (e.g., 7.5; summer
639 to fall, winter). Higher pH values are observed in spring and late fall. While we are lacking the
640 local biological data to sufficiently evaluate past and future ecosystem changes, a high rate of
641 ocean acidification as observed in the Chukchi Sea (Qi et al., 2022b, a), associated with potential
642 temperature-induced shifts in the carbonate chemistry cycle (e.g. Orr et al. 2022), have the
643 potential to impact species and ecosystems. Exposure to low pH increases organismal energy
644 requirements for maintenance (e.g. acid-base regulation: Stumpp et al., 2012, compensatory
645 calcification: Ventura et al., 2016). Organisms can cope with increased energy costs using a
646 variety of strategies, ranging from individual physiological to behavioral responses, depending
647 on trophic level, mobility, and other ecological factors. For example, they can use available
648 stored energy to compensate for increased costs or they can decrease their metabolism to limit
649 costs (AMAP 2018). At the CEO, the low pH period observed during the summer and fall is
650 associated with elevated temperature and an elevated food supply for herbivores (Lalande et al.,
651 2020). The high availability of food may then foster compensation for the higher energetic costs
652 associated with exposure to low pH. However, a longer period of low pH as suggested by our
653 data could lead to a mismatch between the low pH and food availability, with cascading negative
654 consequences for the ecosystem (Kroeker et al., 2021). In winter, the low pH conditions are
655 associated with low temperature, no light, and low food level concentrations. These conditions
656 are likely to keep metabolisms low and limit the negative effects of exposure to low pH
657 (Gianguzza et al., 2014). As food availability is limited by the absence of light, this strategy may

be compromised by an increase in temperature that could also lead to increased metabolism. Additional work is needed to understand impacts of acidification conditions and variability on the marine biota of the Chukchi Sea, including field and laboratory experiments that evaluate biological response under realistic scenarios. The characterization of the environmental conditions at the CEO, including the variability in time, can be used to design single and multiple stressor experiments (carbonate chemistry, temperature, salinity, food, oxygen; Boyd et al. 2018).

Indigenous communities are at the forefront of the changing Arctic, including changes in accessibility, availability, and condition of traditional marine foods (Buschman and Sudlovenick, 2022; Hauser et al., 2021). Several marine species are critical to the food and cultural security of coastal Inupiat who have thrived in Arctic Alaska for millenia. While it is not possible to resolve the consequences of the seasonal and interannual variations in carbonate chemistry documented in this manuscript without a proper sensitivity evaluation, the seasonally low pH conditions have the potential to impact organisms like bivalves in a foraging hotspot for walrus (Jay et al., 2012; Kuletz et al., 2015). Walrus, as well as their bivalve stomach contents, are important nutritional, spiritual, and cultural components, raising concerns for food security in the context of ecosystem shifts associated with the variability and multiplicity of climate impacts within the region (ICC, 2015).

5. Concluding Thoughts

The Chukchi Sea is undergoing a rapid environmental transformation with potentially far-reaching consequences across the ecosystem. While we are lacking a long-term time-series, we used this dataset to investigate the drivers of extreme pH, Ω_{arag}, and pCO_2 and document

conditions that could affect the ecological niches of organisms, including a fast rate of ocean acidification, elongated sea ice free periods, increased primary productivity and elevated temperature. While a combination of experimental and monitoring approaches is needed for an understanding of the ecological consequences of these changes, our results also highlight the urgency to mitigate CO_2 emissions and simultaneously support Indigenous-led conservation measures to safeguard an ecosystem in transition. Indigenous People in the Arctic have established strategies to monitor, adapt to, and conserve the ecosystems upon which they depend. Ethical and equitable engagement of Indigenous Knowledge and the communities at the forefront of climate impacts can help guide research and conservation action by centering local priorities and traditional practices, thereby supporting self-determination and sovereignty (Buschman and Sudlovenick, 2022).

Data availability

The inorganic carbon data used in this manuscript are publicly available (Hauri and Irving, 2023a; Hauri and Irving, 2023b).

Author contributions

CH and BI managed and serviced the HydroC CO_2 and SeapHOx sensors, analyzed and published the data, and wrote the manuscript. SD and Peter Shipton carried out the CEO mooring deployments and recoveries and managed and serviced the CTD and NO_3 sensors. RP, DH, SD, and SLD contributed to the manuscript.

Competing interests

The authors have no competing interests.

Acknowledgments

The Chukchi Ecosystem Observatory is located on the traditional and contemporary hunting grounds of the Northern Alaska Iñupiat. We also acknowledge that our Fairbanks-based offices are located on the Native lands of the Lower Tanana Dena. The Indigenous Peoples of this land never surrendered lands or resources to Russia or the United States. We acknowledge this not only because we are grateful to the Indigenous communities who have been in deep connection with the land and water for time immemorial, but also in recognition of the historical and ongoing legacy of colonialism. We are committed to improving our scientific approaches and working towards co-production for a better future for everyone.

We acknowledge the World Climate Research Programme, which, through its Working Group on Coupled Modelling, coordinated and promoted CMIP6. We thank the climate modeling groups for producing and making available their model output, the Earth System Grid Federation (ESGF) for archiving the data and providing access, and the multiple funding agencies who support CMIP6 and ESGF.

Financial support

We would like to thank the National Pacific Research Board Long-term Monitoring (NPRB LTM) program (project no. 1426 and L-36), the Alaska Ocean Observing System (award no. NA11NOS0120020 and NA16NOS0120027), and the University of Alaska Fairbanks for their financial support. Claudine Hauri, Brita Irving, and Seth Danielson also acknowledge support from the National Science Foundation Office of Ocean Sciences and Polar Programs

(OCE-1841948 and OPP-1603116). Projects that assisted in the servicing of the CEO and/or collected water column calibration data were funded by the National Science Foundation, Bureau of Ocean Energy Management, National Oceanic and Atmospheric Administration, National Oceanographic Partnership Program, and Shell Exploration and Production Company, Inc. Maintenance and calibration of the CEO sensors is only possible due to the kind support of numerous collaborators within the Arctic research community who helped with CEO deployment and recovery or collected sensor calibration samples. We would therefore like to thank Peter Shipton, Carin Ashjian, Jessica Cross, Miguel Goñi, Jackie Grebmeier, Burke Hales, Katrin Iken, Laurie Juranek, Calvin Mordy, and Robert Pickart.

References

Alin, S. R., Feely, R. A., Dickson, A. G., Hernández-Ayón, J. M., Juranek, L. W., Ohman, M. D., and Goericke, R.: Robust empirical relationships for estimating the carbonate system in the southern California Current System and application to CalCOFI hydrographic cruise data (2005–2011), Journal of Geophysical Research, 117, C05033, doi:10.1029/2011JC007511, 2012.

AMAP. AMAP Assessment 2018: Arctic Ocean Acidification. Arctic Monitoring and Assessment Programme (AMAP), Tromsø, Norway. vi+187pp, https://www.amap.no/documents/doc/AMAP-Assessment-2018-Arctic-Ocean-Acidification/1659, 2018.

Arrigo, K. R. and van Dijken, G. L.: Continued increases in Arctic Ocean primary production, Prog. Oceanogr., 136, 60–70, https://doi.org/10.1016/j.pocean.2015.05.002, 2015.

Asahara, Y., Takeuchi, F., Nagashima, K., Harada, N., Yamamoto, K., Oguri, K., and Tadai, O.: Provenance of terrigenous detritus of the surface sediments in the Bering and Chukchi Seas as derived from Sr and Nd isotopes: Implications for recent climate change in the Arctic regions, Deep Sea Res. Part II Top. Stud. Oceanogr., 61–64, 155–171, https://doi.org/10.1016/j.dsr2.2011.12.004, 2012.

Bates, N.: Assessing ocean acidification variability in the Pacific-Arctic region as part of the Russian-American Long-term Census of the Arctic, Oceanography, 28, 36–45, https://doi.org/10.5670/oceanog, 2015.

Bates, N. R., Mathis, J. T. and Cooper, L. W.: Ocean acidification and biologically induced seasonality of carbonate mineral saturation states in the western Arctic Ocean. J. Geophys. Res. 114, 2008JC004862, 2009.

Bednaršek, N., Calosi, P., Feely, R. A., Ambrose, R., Byrne, M., Chan, K. Y. K., Dupont, S., Padilla-Gamiño, J. L., Spicer, J. I., Kessouri, F., Roethler, M., Sutula, M., and Weisberg, S. B.: Synthesis of thresholds of ocean acidification impacts on echinoderms, Front. Mar. Sci., 8, https://doi.org/10.3389/fmars.2021.602601, 2021.

Bittig, H. C., Steinhoff, T., Claustre, H., Fiedler, B., Williams, N. L., Sauzède, R., Körtzinger, A., and Gattuso, J.-P.: An alternative to static climatologies: robust estimation of open ocean

772 CO_2 variables and nutrient concentrations from T, S, and O_2 data using Bayesian neural
773 networks, Front. Mar. Sci., 5, 328, https://doi.org/10.3389/fmars.2018.00328, 2018.
774
775 Blanchard, A. L., Parris, C. L., Knowlton, A. L. and Wade, N. R.: Benthic ecology of the
776 northeastern Chukchi Sea. Part I. Environmental characteristics and macrofaunal community
777 structure, 2008–2010. Continental Shelf Research 67, 52–66, 2013.
778
779 Boucher, O., Denvil, S., Levavasseur, G., Cozic, A., Caubel, A., Foujols, M.-A., Meurdesoif, Y.,
780 Balkanski, Y., Checa-Garcia, R., Hauglustaine, D., Bekki, S. and Marchand, M.: IPSL IPSL-
781 CM6A-LR-INCA model output prepared for CMIP6 AerChemMIP.
782 doi:10.22033/ESGF/CMIP6.13581, 2020.
783
784 Boyd, P. W., Collins, S., Dupont, S., Fabricius, K., Gattuso, J.-P., Havenhand, J., Hutchins, D.
785 A., Riebesell, U., Rintoul, M. S., Vichi, M., Biswas, H., Ciotti, A., Gao, K., Gehlen, M., Hurd, C.
786 L., Kurihara, H., McGraw, C. M., Navarro, J. M., Nilsson, G. E., Passow, U. and Pörtner, H.-O.:
787 Experimental strategies to assess the biological ramifications of multiple drivers of global ocean
788 change—A review. Global Change Biology 24, 2239–2261, 2018.
789
790 Breitberg, D., Salisbury, J., Bernhard, J., Cai, W.-J., Dupont, S., Doney, S., Kroeker,
791 K., Levin, L.A., Long, W. C., Milke, L.M., Miller S.H., Phelan, B., Passow, U., Seibel,
792 B.A., Todgham, A.E., and Tarrant, A.M.: And on top of all that… Coping with ocean
793 acidification in the midst of many stressors. Oceanography, 25(2), 48–61.
794 https://doi.org/10.5670/oceanog.2015.31, 2015.

Bresnahan, P. J., Martz, T. R., Takeshita, Y., Johnson, K. S., and LaShomb, M.: Best practices for autonomous measurement of seawater pH with the Honeywell Durafet, Methods Oceanogr., 9, 44–60, https://doi.org/10.1016/j.mio.2014.08.003, 2014.

Brodzik, M. J. and K. W. Knowles: "Chapter 5: EASE-Grid: A Versatile Set of Equal-Area Projections and Grids." in Michael F.Goodchild (Ed.) Discrete Global Grids: A Web Book. Santa Barbara, California USA: National Center for Geographic Information & Analysis. https://escholarship.org/uc/item/9492q6sm, 2002.

Buschman, V. Q. and Sudlovenick, E.: Indigenous-led conservation in the Arctic supports global conservation practices, Arctic Science, 9(3): 714-719, https://doi.org/10.1139/as-2022-0025, 2022.

Carmack, E. and Wassmann, P.: Food webs and physical–biological coupling on pan-Arctic shelves: unifying concepts and comprehensive perspectives. Progress in Oceanography, 71(2-4), pp.446-477, 2006.

Carter, B. R., Feely, R. A., Williams, N. L., Dickson, A. G., Fong, M. B., and Takeshita, Y.: Updated methods for global locally interpolated estimation of alkalinity, pH, and nitrate, Methods Limnology and Oceanography, 16(2), 119-131, https://doi.org/10.1002/lom3.10232, 2018.

Chatterjee, S., and Hadi, A. S.: “Influential Observations, High Leverage Points, and Outliers in Linear Regression.” Statistical Science, 1(3), 1986, pp. 379–416, 10.1214/ss/1177013622, 1986.

Corlett, W. B. and Pickart, R. S.: The Chukchi slope current. Progress in Oceanography 153, 50–65, 2017.

Cross, J. N., Mathis, J. T., Bates, N. R., and Byrne, R. H.: Conservative and non-conservative variations of total alkalinity on the Southeastern Bering Sea Shelf, Mar. Chem., 154, 100–112, https://doi.org/10.1016/j.marchem.2013.05.012, 2013.

Cross, J. N., Monacci, N. M., Bell, S. W., Grebmeier, J. M., Mordy, C., Pickart, R. S., Stabeno, and P. J.: Dissolved inorganic carbon (DIC), total alkalinity (TA) and other variables collected from discrete samples and profile observations from United States Coast Guard Cutter (USCGC) Healy cruise HLY1702 (EXPOCODE 33HQ20170826) in the Bering and Chukchi Sea along transect lines in the Distributed Biological Observatory (DBO) from 2017-08-26 to 2017-09-15 (NCEI Accession 0208337). NOAA National Centers for Environmental Information. Dataset. https://doi.org/10.25921/pks4-4p43, 2020a.

Cross, J. N., Monacci, N. M., Bell, S. W., Grebmeier, J. M., Mordy, C., Pickart, R. S., and Stabeno, P. J.: Dissolved inorganic carbon (DIC), total alkalinity (TA) and other parameters collected from discrete sample and profile observations during the USCGC Healy cruise HLY1801 (EXPOCODE 33HQ20180807) in the Bering Sea, Chukchi Sea and Beaufort Sea along transect lines in the Distributed Biological Observatory (DBO) from 2018-08-07 to 2018-

08-24 (NCEI Accession 0221911). NOAA National Centers for Environmental Information. Dataset. https://doi.org/10.25921/xc4b-xh20, 2020b.

Cross, J. N., Monacci, N. M., Bell, S. W., Grebmeier, J. M., Mordy, C., Pickart, Robert S., Stabeno, P.J.: Dissolved inorganic carbon (DIC) and total alkalinity (TA) and other hydrographic and chemical data collected from discrete sample and profile observations during the United States Coast Guard Cutter (USCGC) Healy cruise HLY1901 (EXPOCODE 33HQ20190806) in the Bering and Chukchi Sea along transect lines in the Distributed Biological Observatory (DBO) from 2019-08-06 to 2019-08-22 (NCEI Accession 0243277). NOAA National Centers for Environmental Information. Dataset. https://doi.org/10.25921/b5s5-py61, 2021.

Cullison-Gray, S. E., DeGrandpre, M. D., Moore, T. S., Martz, T. R., Friederich, G. E., and Johnson, K. S.: Applications of in situ pH measurements for inorganic carbon calculations, Mar. Chem., 125, 82–90, https://doi.org/10.1016/j.marchem.2011.02.005, 2011.

Daniel, A., Laës-Huon, A., Barus, C., Beaton, A. D., Blandfort, D., Guigues, N., Knockaert, M., Munaron, D., Salter, I., Woodward, E. M. S., Greenwood, N., and Achterberg, E. P.: Toward a harmonization for using in situ nutrient sensors in the marine environment, Front. Mar. Sci., 6, 773, https://doi.org/10.3389/fmars.2019.00773, 2020.

Danielson, S.L., Iken, K., Hauri, C., Hopcroft, R.R., McDonnell, A.M., Winsor, P., Lalande, C., Grebmeier, J.M., Cooper, L.W., Horne, J.K. and Stafford, K.M.: Collaborative approaches to

multi-disciplinary monitoring of the Chukchi shelf marine ecosystem: Networks of networks for maintaining long-term Arctic observations. In OCEANS 2017-Anchorage (pp. 1-7). IEEE, 2017.

Danielson, S. L., Ahkinga, O., Ashjian, C., Basyuk, E., Cooper, L. W., Eisner, L., Farley, E., Iken, K. B., Grebmeier, J. M., Juranek, L., Khen, G., Jayne, S. R., Kikuchi, T., Ladd, C., Lu, K., McCabe, R. M., Moore, G. W. K., Nishino, S., Ozenna, F., Pickart, R. S., Polyakov, I., Stabeno, P. J., Thoman, R., Williams, W. J., Wood, K., and Weingartner, T. J.: Manifestation and consequences of warming and altered heat fluxes over the Bering and Chukchi Sea continental shelves, Deep Sea Res. Part II Top. Stud. Oceanogr., 177, 104781, https://doi.org/10.1016/j.dsr2.2020.104781, 2020.

Danielson, S.: Water temperature, conductivity, and others taken by CTD and Niskin bottles from the research vessel Norseman II Data for Arctic Marine Biodiversity Observing Network, AMBON, Program in the Chukchi Sea from 2017-08-07 to 2017-08-22 (NCEI Accession 0229072). NOAA National Centers for Environmental Information. Dataset. https://doi.org/10.25921/afz7-0d98, 2021.

DeGrandpre, M. D., Lai, C.-Z., Timmermans, M.-L., Krishfield, R. A., Proshutinsky, A. and Torres, D.: Inorganic Carbon and pCO_2 Variability During Ice Formation in the Beaufort Gyre of the Canada Basin. Journal of Geophysical Research: Oceans 124, 4017–4028, 2019.

884 Dickson, A. G.: Thermodynamics of the dissociation of boric acid in synthetic seawater from
885 273.15 to 318.15 K, Deep Sea Res. Part Oceanogr. Res. Pap., 37, 755–766,
886 https://doi.org/10.1016/0198-0149(90)90004-F, 1990.
887
888 Dickson, A. G., Sabine, C. L., and Christian, J. R.: Guide to best practices for ocean CO_2
889 measurements, PICES, Sydney, 191 pp., 2007.
890
891 DiGirolamo, N. E., C. L. Parkinson, D. J. Cavalieri, P. Gloersen, and H. J. Zwally: Sea Ice
892 Concentrations from Nimbus-7 SMMR and DMSP SSM/I-SSMIS Passive Microwave Data,
893 Version 2. Boulder, Colorado USA. NASA National Snow and Ice Data Center Distributed
894 Active Archive Center. https://doi.org/10.5067/MPYG15WAA4WX, 2022.
895
896 Dorey, N., Lançon, P., Thorndyke, M., and Dupont, S.: Assessing physiological tipping point of
897 sea urchin larvae exposed to a broad range of pH, Glob. Change Biol., 19, 3355–3367,
898 https://doi.org/10.1111/gcb.12276, 2013.
899
900 Doney, S. C., Busch, D. S., Cooley, S. R. and Kroeker, K. J.: The Impacts of Ocean
901 Acidification on Marine Ecosystems and Reliant Human Communities. Annu. Rev. Environ.
902 Resour. 45, 83–112, 2020.
903
904 Duke, P. J., Else, B. G. T., Jones, S. F., Marriot, S., Ahmed, M. M. M., Nandan, V., Butterworth,
905 B., Gonski, S. F., Dewey, R., Sastri, A., Miller, L. A., Simpson, K. G., and Thomas, H.: Seasonal
906 marine carbon system processes in an Arctic coastal landfast sea ice environment observed with

907 an innovative underwater sensor platform, Elementa: Science of the Anthropocene, 9 (1): 00103,
908 https://doi.org/10.1525/elementa.2021.00103, 2021.
909
910 Etminan, M., Myhre, G., Highwood, E. J., and Shine, K. P.: Radiative forcing of carbon dioxide,
911 methane, and nitrous oxide: A significant revision of the methane radiative forcing, Geophys.
912 Res. Lett., 43, 12,614-12,623, https://doi.org/10.1002/2016GL071930, 2016.
913
914 Fang, Y.C., Weingartner, T.J., Dobbins, E.L., Winsor, P., Statscewich, H., Potter, R.A., Mudge,
915 T.D., Stoudt, C.A. and Borg, K.: Circulation and thermohaline variability of the Hanna Shoal
916 region on the northeastern Chukchi Sea shelf. Journal of Geophysical Research: Oceans, 125(7),
917 p.e2019JC015639, 2020.
918
919 Fietzek, P., Fiedler, B., Steinhoff, T., and Körtzinger, A.: In situ quality assessment of a novel
920 underwater CO_2 sensor based on membrane equilibration and NDIR spectrometry, J.
921 Atmospheric Ocean. Technol., 31, 181–196, https://doi.org/10.1175/JTECH-D-13-00083.1,
922 2014.
923
924 Friis, K.: The salinity normalization of marine inorganic carbon chemistry data, Geophys. Res.
925 Lett., 30, 1085, https://doi.org/10.1029/2002GL015898, 2003.
926
927 Gianguzza, P., Visconti, G., Gianguzza, F., Vizzini, S., Sarà, G., and Dupont, S.: Temperature
928 modulates the response of the thermophilous sea urchin Arbacia lixula early life stages to CO_2-

929 driven acidification, Mar. Environ. Res., 93, 70–77,
930 https://doi.org/10.1016/j.marenvres.2013.07.008, 2014.
931
932 Goethel, C. L., Grebmeier, J. M., Cooper, L. W., and Miller, T. J.: Implications of ocean
933 acidification in the Pacific Arctic: Experimental responses of three Arctic bivalves to decreased
934 pH and food availability, Deep Sea Res. Part II Top. Stud. Oceanogr., 144, 112–124,
935 https://doi.org/10.1016/j.dsr2.2017.08.013, 2017.
936
937 Gonzalez, S., Horne, J. K., and Danielson, S. L.: Multi-scale temporal variability in biological-
938 physical associations in the NE Chukchi Sea, Polar Biol., 44, 837–855,
939 https://doi.org/10.1007/s00300-021-02844-1, 2021.
940
941 Grebmeier, J. M., Bluhm, B. A., Cooper, L. W., Danielson, S. L., Arrigo, K. R., Blanchard, A.
942 L., Clarke, J. T., Day, R. H., Frey, K. E., Gradinger, R. R., Kędra, M., Konar, B., Kuletz, K. J.,
943 Lee, S. H., Lovvorn, J. R., Norcross, B. L. and Okkonen, S. R.: Ecosystem characteristics and
944 processes facilitating persistent macrobenthic biomass hotspots and associated benthivory in the
945 Pacific Arctic. Progress in Oceanography 136, 92–114,
946 https://doi.org/10.1016/j.pocean.2015.05.006, 2015.
947
948 Hauri, C., Gruber, N., Vogt, M., Doney, S. C., Feely, R. A., Lachkar, Z., Leinweber, A.,
949 McDonnell, A. M. P., Munnich, M. and Plattner, G.-K.: Spatiotemporal variability and long-term
950 trends of ocean acidification in the California Current System. Biogeosciences 10, 193–216,
951 https://doi.org/10.5194/bg-10-193-2013, 2013.

Hauri, C., Danielson, S., McDonnell, A. M. P., Hopcroft, R. R., Winsor, P., Shipton, P., Lalande, C., Stafford, K. M., Horne, J. K., Cooper, L. W., Grebmeier, J. M., Mahoney, A., Maisch, K., McCammon, M., Statscewich, H., Sybrandy, A., and Weingartner, T.: From sea ice to seals: a moored marine ecosystem observatory in the Arctic, Ocean Sci., 14, 1423–1433, https://doi.org/10.5194/os-14-1423-2018, 2018.

Hauri, C., Pagès, R., McDonnell, A. M. P., Stuecker, M. F., Danielson, S. L., Hedstrom, K., Irving, B., Schultz, C., and Doney, S. C.: Modulation of ocean acidification by decadal climate variability in the Gulf of Alaska, Communications Earth & Environment 2, 191, https://doi.org/10.1038/s43247-021-00254-z, 2021.

Hauri, C. and Irving, B.: pCO_2 time series measurements from the Chukchi Ecosystem Observatory CEO2 mooring deployed at 33 meters depth in the Northeast Chukchi Sea. Research Workspace. https://doi.org/10.24431/rw1k7dq, version: 10.24431_rw1k7dq_20230531T123002Z, 2023a.

Hauri, C. and Irving, B.: pH, temperature, salinity, and oxygen time series measurements from the Chukchi Ecosystem Observatory CEO2 mooring deployed at 33 meters depth in the Northeast Chukchi Sea. Research Workspace. https://doi.org/10.24431/rw1k7dp, version: 10.24431_rw1k7dp_20230531T121136Z, 2023b.

974 Hauser, D. D. W., Whiting, A. V., Mahoney, A. R., Goodwin, J., Harris, C., Schaeffer, R. J.,
975 Schaeffer, R., Laxague, N. J. M., Subramaniam, A., Witte, C. R., Betcher, S., Lindsay, J. M., and
976 Zappa, C. J.: Co-production of knowledge reveals loss of Indigenous hunting opportunities in the
977 face of accelerating Arctic climate change, Environ. Res. Lett., 16, 095003,
978 https://doi.org/10.1088/1748-9326/ac1a36, 2021.
979
980 Hayes, D., Kemme, J., and Hauri C.: Ocean greenhouse gas monitoring: new autonomous
981 platform to measure pCO_2, methane, Sea Technology, 63(10), 13-16, https://lsc-
982 pagepro.mydigitalpublication.com/publication/?i=764237&p=13&view=issueViewer, 2022.
983
984 Hennon, T. D., Danielson, S. L., Woodgate, R. A., Irving, B., Stockwell, D. A., and Mordy, C.
985 W.: Mooring Measurements of Anadyr Current Nitrate, Phosphate, and Silicate Enable Updated
986 Bering Strait Nutrient Flux Estimates, Geophys. Res. Lett., 49, e2022GL098908,
987 https://doi.org/10.1029/2022GL098908, 2022.
988
989 Holmes, R.M., J.W. McClelland, S.E. Tank, R.G.M. Spencer, and A.I. Shiklomanov.: Arctic
990 Great Rivers Observatory. Water Quality Dataset, https://www.arcticgreatrivers.org/data, 2021.
991
992 Horowitz, L. W., Naik, V., Sentman, L., Paulot, F., Blanton, C., McHugh, C., Radhakrishnan, A.,
993 Rand, K., Vahlenkamp, H., Zadeh, N. T., Wilson, C., Ginoux, P., He, J., John, J. G., Lin, M.,
994 Paynter, D. J., Ploshay, J., Zhang, A. and Zeng, Y.: NOAA-GFDL GFDL-ESM4 model output
995 prepared for CMIP6 AerChemMIP hist-1950HC. doi:10.22033/ESGF/CMIP6.8568, 2018.
996

997 Huntington, H. P., Danielson, S. L., Wiese, F. K., Baker, M., Boveng, P., Citta, J. J., De
998 Robertis, A., Dickson, D. M. S., Farley, E., George, J. C., Iken, K., Kimmel, D. G., Kuletz, K.,
999 Ladd, C., Levine, R., Quakenbush, L., Stabeno, P., Stafford, K. M., Stockwell, D., and Wilson,
1000 C.: Evidence suggests potential transformation of the Pacific Arctic ecosystem is underway, Nat.
1001 Clim. Change, 10, 342–348, https://doi.org/10.1038/s41558-020-0695-2, 2020.
1002
1003 Huntington, H. P., Zagorsky, A., Kaltenborn, B. P., Shin, H. C., Dawson, J., Lukin, M., Dahl, P.
1004 E., Guo, P., and Thomas, D. N.: Societal implications of a changing Arctic Ocean. Ambio, 51(2),
1005 298–306. https://doi.org/10.1007/s13280-021-01601-2, 2022.
1006
1007 ICC: Alaskan Inuit food security conceptual framework: how to assess the Arctic from an Inuit
1008 perspective, Inuit Circumpolar Council-Alaska, Anchorage, 2015.
1009
1010 Irving, B., SUNA_V2_processing, GitHub repository, https://github.com/britairving/SUNA_V2,
1011 2021.
1012
1013 Islam, F., DeGrandpre, M. D., Beatty, C.M., Timmermanns, M.-L., Krishfield, R. A., Toole,
1014 J.M., and Laney, S.R.: Sea surface pCO_2 and O_2 dynamics in the partially ice-covered Arctic
1015 Ocean, JGR Oceans, 122(2), 1425-1438, https://doi.org/10.1002/2016JC012162, 2017.
1016
1017 Jay, C. V., Fischbach, A. S., and Kochnev, A. A.: Walrus areas of use in the Chukchi Sea during
1018 sparse sea ice cover, Mar. Ecol. Prog. Ser., 468, 1–13, https://doi.org/10.3354/meps10057, 2012.
1019

Jiang, L.-Q., Feely, R. A., Wanninkhof, R., Greeley, D., Barbero, L., Alin, S., Carter, B. R., Pierrot, D., Featherstone, C., Hooper, J., Melrose, C., Monacci, N., Sharp, J. D., Shellito, S., Xu, Y.-Y., Kozyr, A., Byrne, R. H., Cai, W.-J., Cross, J., Johnson, G. C., Hales, B., Langdon, C., Mathis, J., Salisbury, J., and Townsend, D. W.: Coastal Ocean Data Analysis Product in North America (CODAP-NA) – an internally consistent data product for discrete inorganic carbon, oxygen, and nutrients on the North American ocean margins, Earth Syst. Sci. Data, 13, 2777–2799, https://doi.org/10.5194/essd-13-2777-2021, 2021.

Jung, J., Son, J. E., Lee, Y. K., Cho, K.-H., Lee, Y., Yang, E. J., Kang, S.-H., and Hur, J.: Tracing riverine dissolved organic carbon and its transport to the halocline layer in the Chukchi Sea (western Arctic Ocean) using humic-like fluorescence fingerprinting, Sci. Total Environ., 772, 145542, https://doi.org/10.1016/j.scitotenv.2021.145542, 2021.

Juranek, L. W., Feely, R. A., Peterson, W. T., Alin, S. R., Hales, B., Lee, K., Sabine, C. L., and Peterson, J.: A novel method for determination of aragonite saturation state on the continental shelf of central Oregon using multi-parameter relationships with hydrographic data, Geophys. Res. Lett., 36, L24601, https://doi.org/10.1029/2009GL040778, 2009.

Juranek, L. W., Feely, R. A., Gilbert, D., Freeland, H., and Miller, L. A.: Real-time estimation of pH and aragonite saturation state from Argo profiling floats: Prospects for an autonomous carbon observing strategy, Geophys. Res. Lett., 38, L17603, https://doi.org/10.1029/2011gl048580, 2011.

1043 Koch, C. W., Cooper, L. W., Lalande, C., Brown, T. A., Frey, K. E. and Grebmeier, J. M.:
1044 Seasonal and latitudinal variations in sea ice algae deposition in the Northern Bering and
1045 Chukchi Seas determined by algal biomarkers. PLoS ONE 15, e0231178, 2020.
1046
1047 Kroeker, K. J., Powell, C., and Donham, E. M.: Windows of vulnerability: Seasonal mismatches
1048 in exposure and resource identity determine ocean acidification's effect on a primary consumer
1049 at high latitude, Glob. Change Biol., 27, 1042–1051, https://doi.org/10.1111/gcb.15449, 2021.
1050
1051 Kuletz, K. J., Ferguson, M. C., Hurley, B., Gall, A. E., Labunski, E. A., and Morgan, T. C.:
1052 Seasonal spatial patterns in seabird and marine mammal distribution in the eastern Chukchi and
1053 western Beaufort seas: Identifying biologically important pelagic areas, Prog. Oceanogr., 136,
1054 175–200, https://doi.org/10.1016/j.pocean.2015.05.012, 2015.
1055
1056 Lalande, C., Grebmeier, J. M., Hopcroft, R. R., and Danielson, S. L.: Annual cycle of export
1057 fluxes of biogenic matter near Hanna Shoal in the northeast Chukchi Sea, Deep Sea Res. Part II
1058 Top. Stud. Oceanogr., 177, 104730, https://doi.org/10.1016/j.dsr2.2020.104730, 2020.
1059
1060 Lalande, C., Grebmeier, J. M., McDonnell, A. M. P., Hopcroft, R. R., O'Daly, S., and Danielson,
1061 S. L.: Impact of a warm anomaly in the Pacific Arctic region derived from time-series export
1062 fluxes, PLOS ONE, 16, e0255837, https://doi.org/10.1371/journal.pone.0255837, 2021.
1063
1064 Lauvset, S. K., Lange, N., Tanhua, T., Bittig, H. C., Olsen, A., Kozyr, A., Álvarez, M., Becker,
1065 S., Brown, P. J., Carter, B. R., Cotrim da Cunha, L., Feely, R. A., van Heuven, S., Hoppema, M.,

Ishii, M., Jeansson, E., Jutterström, S., Jones, S. D., Karlsen, M. K., Lo Monaco, C., Michaelis, P., Murata, A., Pérez, F. F., Pfeil, B., Schirnick, C., Steinfeldt, R., Suzuki, T., Tilbrook, B., Velo, A., Wanninkhof, R., Woosley, R. J., and Key, R. M.: An updated version of the global interior ocean biogeochemical data product, GLODAPv2.2021, Earth Syst. Sci. Data Discuss., https://doi.org/10.5194/essd-2021-234, 2021.

Laws, E. A.: Photosynthetic quotients, new production and net community production in the open ocean, Deep Sea Res. Part Oceanogr. Res. Pap., 38, 143–167, https://doi.org/10.1016/0198-0149(91)90059-O, 1991.

Lee, K., Kim, T.-W., Byrne, R. H., Millero, F. J., Feely, R. A., and Liu, Y.-M.: The universal ratio of boron to chlorinity for the North Pacific and North Atlantic oceans, Geochim. Cosmochim. Acta, 74, 1801–1811, https://doi.org/10.1016/j.gca.2009.12.027, 2010.

Lewis, E. and Wallace, D. W. R.: Program Developed for CO2 System Calculations, ORNL/CDIAC-105, Carbon Dioxide Inf. Anal. Cent., Oak Ridge Natl. Lab., Oak Ridge, Tenn., 38 pp., https://salish-sea.pnnl.gov/media/ORNL-CDIAC-105.pdf, 1998.

Lewis, K. M., van Dijken, G. L., and Arrigo, K. R.: Changes in phytoplankton concentration now drive increased Arctic Ocean primary production, Science, 369, 198–202, https://doi.org/10.1126/science.aay8380, 2020.

Li, B., Watanabe, Y. W., and Yamaguchi, A.: Spatiotemporal distribution of seawater pH in the North Pacific subpolar region by using the parameterization technique, J. Geophys. Res. Oceans, 121, 3435–3449, https://doi.org/10.1002/2015JC011615, 2016.

Licker, R., Ekwurzel, B., Doney, S. C., Cooley, S. R., Lima, I. D., Heede, R., and Frumhoff, P. C.: Attributing ocean acidification to major carbon producers, Environ. Res. Lett., 14, 124060, https://doi.org/10.1088/1748-9326/ab5abc, 2019.

Lueker, T. J., Dickson, A. G., and Keeling, C. D.: Ocean pCO_2 calculated from dissolved inorganic carbon, alkalinity, and equations for K 1 and K 2: validation based on laboratory measurements of CO_2 in gas and seawater at equilibrium, Mar. Chem., 70, 105–119, https://doi.org/10.1016/S0304-4203(00)00022-0, 2000.

Mathis, J. T. and Questel, J. M.: Assessing seasonal changes in carbonate parameters across small spatial gradients in the Northeastern Chukchi Sea. Continental Shelf Research 67, 42–51, https://doi.org/10.1016/j.csr.2013.04.041, 2013.

Martz, T. R., Connery, J. G., and Johnson, K. S.: Testing the Honeywell Durafet for seawater pH applications, Limnol. Oceanogr. Methods, 8, 172–184, https://doi.org/10.4319/lom.2010.8.172, 2010.

Mauritsen, T., Bader, J., Becker, T., Behrens, J., Bittner, M., Brokopf, R., Brovkin, V., Claussen, M., Crueger, T., Esch, M., Fast, I., Fiedler, S., Fläschner, D., Gayler, V., Giorgetta, M., Goll, D.

S., Haak, H., Hagemann, S., Hedemann, C., Hohenegger, C., Ilyina, T., Jahns, T., Jimenéz-de-la-Cuesta, D., Jungclaus, J., Kleinen, T., Kloster, S., Kracher, D., Kinne, S., Kleberg, D., Lasslop, G., Kornblueh, L., Marotzke, J., Matei, D., Meraner, K., Mikolajewicz, U., Modali, K., Möbis, B., Müller, W. A., Nabel, J. E. M. S., Nam, C. C. W., Notz, D., Nyawira, S.-S., Paulsen, H., Peters, K., Pincus, R., Pohlmann, H., Pongratz, J., Popp, M., Raddatz, T. J., Rast, S., Redler, R., Reick, C. H., Rohrschneider, T., Schemann, V., Schmidt, H., Schnur, R., Schulzweida, U., Six, K. D., Stein, L., Stemmler, I., Stevens, B., von Storch, J.-S., Tian, F., Voigt, A., Vrese, P., Wieners, K.-H., Wilkenskjeld, S., Winkler, A., and Roeckner, E.: Developments in the MPI-M Earth System Model version 1.2 (MPI-ESM1.2) and Its Response to Increasing CO_2, J. Adv. Model. Earth Syst., 11, 998–1038, https://doi.org/10.1029/2018MS001400, 2019.

McDougall, T.J. and Barker, P.M.: Getting started with TEOS-10 and the Gibbs Seawater (GSW) Oceanographic Toolbox, 28pp., SCOR/IAPSO WG127, ISBN 978-0-646-55621-5, 2011.

McRaven, L. and Pickart, R.: Conductivity-Temperature-Depth (CTD) data from the 2018 Distributed Biological Observatory - Northern Chukchi Integrated Study (DBO-NCIS) cruise on USCGC (US Coast Guard Cutter) Healy (HLY1801). Arctic Data Center. doi:10.18739/A2HT2GC7Z, 2021.

Monacci, N. M., Cross, J. N., Pickart, R. S., Juranek, L. W., McRaven, L. T., and Becker, S.: Dissolved inorganic carbon (DIC) and total alkalinity (TA) and other hydrographic and chemical data collected from discrete sample and profile observations aboard the RV Sikuliaq Cruise SKQ202014S (EXPOCODE 33BI20201025) in the Bering and Chukchi Sea along transect lines

in the Distributed Biological Observatory (DBO) from 2020-10-25 to 2020-11-11 (NCEI Accession 0252613). NOAA National Centers for Environmental Information. Dataset. https://doi.org/10.25921/pnsd-sv10, 2022.

Moore, S. E., Douglas P. deMaster, and Paul K. Dayton: Cetacean Habitat Selection in the Alaskan Arctic during Summer and Autumn, Arctic, 53(4), 432–47. JSTOR, http://www.jstor.org/stable/40512256, 2000.

Moore, S. E., and Stabeno, P. J.: Synthesis of Arctic Research (SOAR) in marine ecosystems of the Pacific Arctic, Progress in Oceanography, 136, 1-11, https://doi.org/10.1016/j.pocean.2015.05.017, 2015,

Moore, S. E., Clarke, J. T., Okkonen, S. R., Grebmeier, J. M., Berchok, C. L., and Stafford, K. M.: Changes in gray whale phenology and distribution related to prey variability and ocean biophysics in the northern Bering and eastern Chukchi seas. PLOS ONE 17(4): e0265934. https://doi.org/10.1371/journal.pone.0265934, 2022.

Mordy, C. W., Bell, S., Cokelet, E. D., Ladd, C., Lebon, G., Proctor, P., Stabeno, P., Strausz, D., Wisegarver, E., and Wood, K.: Seasonal and interannual variability of nitrate in the eastern Chukchi Sea: Transport and winter replenishment, Deep-Sea Res. Part II Top. Stud. Oceanogr., 177, 104807, https://doi.org/10.1016/j.dsr2.2020.104807, 2020.

National Academies of Sciences, Engineering and Medicine: Valuing Climate Damages: Updating Estimation of the Social Cost of Carbon Dioxide (Washington DC: The National Academies Press) https://doi.org/10.17226/24651, 2017.

Newton, J. A., Feely, R. A., Jewett, E. B., Williamson, P., and Mathis, J.: Global ocean acidification observing network: requirements and governance plan, GOA-ON, Washington, 61 pp., http://www.goa-on.org/docs/GOA-ON_plan_print.pdf, 2015.

Orr, J. C.: Recent and future changes in ocean carbonate chemistry, in: Ocean acidification, edited by: Gattuso, J.-P. and Hansson, L., Oxford University Press, Oxford, 41–66, 2011.

Orr, J. C., Epitalon, J.-M., Dickson, A. G., and Gattuso, J.-P.: Routine uncertainty propagation for the marine carbon dioxide system, Mar. Chem., 207, 84–107, https://doi.org/10.1016/j.marchem.2018.10.006, 2018.

Orr, J. C., Kwiatkowski, L., and Pörtner, H. O.: Arctic Ocean annual high in pCO_2 could shift from winter to summer, Nature, 610, 94–100, https://doi.org/10.1038/s41586-022-05205-y, 2022.

Ouyang, Z., Collins, A., Li, Y., Qi, D., Arrigo, K. R., Zhuang, Y., Nishino, S., Humphreys, M. P., Kosugi, N., Murata, A., Kirchman, D. L., Chen, L., Chen, J. and Cai, W.-J.: Seasonal Water Mass Evolution and Non-Redfield Dynamics Enhance CO_2 Uptake in the Chukchi Sea. Journal of Geophysical Research: Oceans 127, e2021JC018326,

https://doi.org/10.1029/2021JC018326, 2022.

Payne, C. M., Bianucci, L., van Dijken, G. L., and Arrigo, K. R.: Changes in Under-Ice Primary Production in the Chukchi Sea From 1988 to 2018, J. Geophys. Res. Oceans, 126, e2021JC017483, https://doi.org/10.1029/2021JC017483, 2021.

Perez, F. F. and Fraga, F.: Association constant of fluoride and hydrogen ions in seawater, Mar. Chem., 21, 161–168, https://doi.org/10.1016/0304-4203(87)90036-3, 1987.

Pipko, I. I., Semiletov, I. P., Tishchenko, P. Y., Pugach, S. P. and Christensen, J. P.: Carbonate chemistry dynamics in Bering Strait and the Chukchi Sea. Progress in Oceanography 55, 77–94, https://doi.org/10.1016/S0079-6611(02)00071-X,2 002.

Qi, D., Chen, L., Chen, B., Gao, Z., Zhong, W., Feely, R. A., Anderson, L. G., Sun, H., Chen, J., Chen, M., Zhan, L., Zhang, Y., and Cai, W.-J.: Increase in acidifying water in the western Arctic Ocean, Nat. Clim. Change, 7, 195–199, https://doi.org/10.1038/nclimate3228, 2017.

Qi, D., Ouyang, Z., Chen, L., Wu, Y., Lei, R., Chen, B., Feely, R. A., Anderson, L. G., Zhong, W., Lin, H., Polukhin, A., Zhang, Y., Zhang, Y., Bi, H., Lin, X., Luo, Y., Zhuang, Y., He, J., Chen, J., and Cai, W. J.: Climate change drives rapid decadal acidification in the Arctic Ocean from 1994 to 2020, Science, 377, 1544–1550, https://doi.org/10.1126/science.abo0383, 2022a.

Qi, D., Wu, Y., Chen, L., Cai, W.-J., Ouyang, Z., Zhang, Y., Anderson, L. G., Feely, R. A., Zhuang, Y., Lin, H., Lei, R., and Bi, H.: Rapid acidification of the Arctic Chukchi Sea waters driven by anthropogenic forcing and biological carbon recycling, Geophysical Research Letter, 49(4), e2021GL097246, **https://doi.org/10.1029/2021GL097246**, 2022b.

Raimondi, L., Matthews, J. B. R., Atamanchuck, D., Azetsu-Scott, K., and Wallace, D.: The internal consistency of the marine carbon dioxide system for high latitude shipboard and in situ monitoring, Mar. Chem., 213, 49–70, https://doi.org/10.1016/j.marchem.2019.03.001, 2019.

Rantanen, M., Karpechko, A. Y., Lipponen, A., Nordling, K., Hyvärinen, O., Ruosteenoja, K., Vihma, T., and Laaksonen, A.: The Arctic has warmed nearly four times faster than the globe since 1979, Commun. Earth Environ., 3, 1–10, https://doi.org/10.1038/s43247-022-00498-3, 2022.

Rheuban, J. E., Doney, S. C., McCorkle, D. C. and Jakuba, R. W. Quantifying the Effects of Nutrient Enrichment and Freshwater Mixing on Coastal Ocean Acidification. Journal of Geophysical Research: Oceans 124(12), 9085–9100, https://doi.org/10.1029/2019JC015556, 2019.

Rysgaard, S., Glud, R. N., Sejr, M. K., Bendtsen, J., and Christensen, P. B.: Inorganic carbon transport during sea ice growth and decay: A carbon pump in polar seas, J. Geophys. Res., 112, C03016, https://doi.org/10.1029/2006JC003572, 2007.

Rysgaard, S., Glud, R. N., Lennert, K., Cooper, M., Halden, N., Leakey, R. J. G., Hawthorne, F. C., and Barber, D.: Ikaite crystals in melting sea ice – implications for pCO_2 and pH levels in Arctic surface waters, The Cryosphere, 6, 901–908, https://doi.org/10.5194/tc-6-901-2012, 2012.

Sakamoto, C. M., Johnson, K. S., and Coletti, L. J.: Improved algorithm for the computation of nitrate concentrations in seawater using an in situ ultraviolet spectrophotometer, Limnol. Oceanogr. Methods, 7, 132–143, https://doi.org/10.4319/lom.2009.7.132, 2009.

Sandy, S. J., Danielson, S. L., and Mahoney, A. R.: Automating the Acoustic Detection and Characterization of Sea Ice and Surface Waves, J. Mar. Sci. Eng., 10, 1577, https://doi.org/10.3390/jmse10111577, 2022.

Sarmiento, J. L. and Gruber, N.: Ocean Biogeochemical Dynamics, Princeton University Press, Princeton, NJ, 526 pp., 2006.

Seabird. Application Note 31: Computing temperature and conductivity slope and offset correction coefficients from lab calibration and salinity bottle samples. my.hach.com/asset-get.download.jsa?id=54627861537, accessed 20 June 2016.

Seabird. Module 28. Advanced Biogeochemical Processing, www.seabird.com/cms-portals/seabird_com/cms/documents/training/Module28_Advanced_Biogeochem_Processing.pdf . Accessed 30 May 2023.

Seferian, R.: CNRM-CERFACS CNRM-ESM2-1 model output prepared for CMIP6 AerChemMIP. doi:10.22033/ESGF/CMIP6.1389, 2019.

Semiletov, I., Pipko, I., Gustafsson, Ö., Anderson, L. G., Sergienko, V., Pugach, S., Dudarev, O., Charkin, A., Gukov, A., Bröder, L., Andersson, A., Spivak, E., and Shakhova, N.: Acidification of East Siberian Arctic Shelf waters through addition of freshwater and terrestrial carbon. Nature Geosci 9, 361–365, https://doi.org/10.1038/ngeo2695, 2016.

Serreze, M. C. and Barry, R. G.: Processes and impacts of Arctic amplification: A research synthesis, Glob. Planet. Change, 77, 85–96, https://doi.org/10.1016/j.gloplacha.2011.03.004, 2011.

Serreze, M. C. and Francis, J. A.: The Arctic amplification debate, Clim. Change, 76, 241–264, https://doi.org/10.1007/s10584-005-9017-y, 2006.

Serreze, M. C., Crawford, A. D., Stroeve, J. C., Barrett, A. P., and Woodgate, R. A.: Variability, trends, and predictability of seasonal sea ice retreat and advance in the Chukchi Sea, J. Geophys. Res. Oceans, 121, 7308–7325, https://doi.org/10.1002/2016JC011977, 2016.

Sharp, J. D., Pierrot, D., Humphreys, M. P., Epitalon, J.-M., Orr, J. C., Lewis, E. R., and Wallace, D. W. R.: CO2SYSv3 for MATLAB, https://doi.org/10.5281/zenodo.7552554, 2023.

Shu, Q., Wang, Q., Årthun, M., Wang, S., Song, Z., Zhang, M., and Qiao, F: Arctic Ocean Amplification in a warming climate in CMIP6 models. Science Advances, 8(30), eabn9755. https://doi.org/10.1126/sciadv.abn9755, 2022.

Stabeno, P. J., Mordy, C. W. and Sigler, M. F.: Seasonal patterns of near-bottom chlorophyll fluorescence in the eastern Chukchi Sea: 2010–2019. Deep Sea Research Part II: Topical Studies in Oceanography 177, 104842, https://doi.org/10.1016/j.dsr2.2020.104842, 2020.

Stackpoole, S., Butman, D., Clow, D., Verdin, K., Gaglioti, B., and Striegl, R. G.: Carbon burial, transport, and emission from inland aquatic ecosystems in Alaska, USGS Prof. Pap., 1826, 159–188, https://doi.org/10.3133/pp1826, 2016.

Stackpoole, S. M., Butman, D., Clow, D. W., Verdin, K. L., Gaglioti, B. V., Genet, H., and Striegl, R. G.: Inland waters and their role in the carbon cycle of Alaska, Ecol. Appl., 27, 1403–1420, http://onlinelibrary.wiley.com/doi/10.1002/eap.1552/full, 2017.

Silvers, L., Blanton, C., McHugh, C., John, J. G., Radhakrishnan, A., Rand, K., Balaji, V., Dupuis, C., Durachta, J., Guo, H., Hemler, R., Lin, P., Nikonov, S., Paynter, D. J., Ploshay, J., Vahlenkamp, H., Wilson, C., Wyman, B., Robinson, T., Zeng, Y. and Zhao, M.: NOAA-GFDL GFDL-CM4 model output prepared for CMIP6 CFMIP. doi:10.22033/ESGF/CMIP6.1641, 2018.

1290 Stroeve, J. C., Serreze, M. C., Holland, M. M., Kay, J. E., Malanik, J., and Barrett, A. P.: The
1291 Arctic's rapidly shrinking sea ice cover: a research synthesis, Clim. Change, 110, 1005–1027,
1292 https://doi.org/10.1007/s10584-011-0101-1, 2011.
1293
1294 Stroeve, J. C., Markus, T., Boisvert, L., Miller, J., and Barrett, A.: Changes in Arctic melt season
1295 and implications for sea ice loss, Geophys. Res. Lett., 41, 1216–1225,
1296 https://doi.org/10.1002/2013GL058951, 2014.
1297
1298 Stumpp, M., Hu, M. Y., Melzner, F., Gutowska, M. A., Dorey, N., Himmerkus, N., Holtmann,
1299 W. C., Dupont, S. T., Thorndyke, M. C., and Bleich, M.: Acidified seawater impacts sea urchin
1300 larvae pH regulatory systems relevant for calcification, Proc. Natl. Acad. Sci. USA, 109, 18192–
1301 18197, https://doi.org/10.1073/pnas.1209174109, 2012.
1302
1303 Sulpis, O., Lauvset, S. K., and Hagens, M.: Current estimates of K_1* and K_2* appear inconsistent
1304 with measured CO_2 system parameters in cold oceanic regions, Ocean Sci., 16, 847–862,
1305 https://doi.org/10.5194/os-16-847-2020, 2020.
1306
1307 Takahashi, T., Sutherland, S. C., Sweeney, C., Poisson, A., Metzl, N., Tilbrook, B., Bates, N.,
1308 Wanninkhof, R., Feely, R. A., Sabine, C., Olafsson, J., and Nojiri, Y.: Global sea–air CO_2 flux
1309 based on climatological surface ocean pCO_2, and seasonal biological and temperature effects,
1310 Deep Sea Res. Part II Top. Stud. Oceanogr., 49, 1601–1622, https://doi.org/10.1016/S0967-
1311 0645(02)00003-6, 2002.
1312

1313 Terhaar, J., Torres, O., Bourgeois, T., and Kwiatkowski, L.: Arctic Ocean acidification over the
1314 21st century co-driven by anthropogenic carbon increases and freshening in the CMIP6 model
1315 ensemble, Biogeosciences, 18, 2221–2240, https://doi.org/10.5194/bg-18-2221-2021, 2021.
1316
1317 Thomsen, J., Casties, I., Pansch, C., Körtzinger, A., and Melzner, F.: Food availability outweighs
1318 ocean acidification effects in juvenile Mytilus edulis: laboratory and field experiments, Glob.
1319 Change Biol., 19, 1017–1027, https://doi.org/10.1111/gcb.12109, 2013.
1320
1321 Thor, P. and Dupont, S.: Transgenerational effects alleviate severe fecundity loss during ocean
1322 acidification in a ubiquitous planktonic copepod, Glob. Change Biol., 21, 2261–2271,
1323 https://doi.org/10.1111/gcb.12815, 2015.
1324
1325 Tian, F., Pickart, R.S., Lin, P., Pacini, A., Moore, G.W.K., Stabeno, P., Weingartner, T., Itoh,
1326 M., Kikuchi, T., Dobbins, E. and Bell, S.: Mean and seasonal circulation of the eastern Chukchi
1327 Sea from moored timeseries in 2013–2014. Journal of Geophysical Research: Oceans, 126(5),
1328 p.e2020JC016863, 2021.
1329
1330 Tunnicliffe, V., Davies, K. T. A., Butterfield, D. A., Embley, R. W., Rose, J. W., and Chadwick
1331 Jr, W. W.: Survival of mussels in extremely acidic waters on a submarine volcano, Nat. Geosci.,
1332 2, 344–348, https://doi.org/10.1038/ngeo500, 2009.
1333
1334 Van Straalen, M. N.: Peer Reviewed: Ecotoxicology Becomes Stress Ecology, Environ. Sci.
1335 Technol., 37, 324A-330A, https://doi.org/10.1021/es0325720, 2003.

Vargas, C. A., Lagos, N. A., Lardies, M. A., Duarte, C., Manríquez, P. H., Aguilera, V. M., Broitman, B., Widdicombe, S., and Dupont, S.: Species-specific responses to ocean acidification should account for local adaptation and adaptive plasticity, Nat Ecol Evol **1**, 0084, https://doi.org/10.1038/s41559-017-0084, 2017.

Vargas, C. A., Cuevas, L. A., Broitman, B. R., San Martin, V. A., Lagos, N. A., Gaitán-Espitia, J. D., and Dupont, S.: Upper environmental pCO_2 drives sensitivity to ocean acidification in marine invertebrates, Nat. Clim. Change, 12, 200–207, https://doi.org/10.1038/s41558-021-01269-2, 2022.

Ventura, A., Schulz, S., and Dupont, S.: Maintained larval growth in mussel larvae exposed to acidified under-saturated seawater, Sci. Rep., 6, 23728, https://doi.org/10.1038/srep23728, 2016.

Vergara-Jara, M. J., DeGrandpre, M. D., Torres, R., Beatty, C. M., Cuevas, L. A., Alarcón, E. and Iriarte, J. L: Seasonal Changes in Carbonate Saturation State and Air-Sea CO_2 Fluxes During an Annual Cycle in a Stratified-Temperate Fjord (Reloncaví Fjord, Chilean Patagonia). Journal of Geophysical Research: Biogeosciences 124, 2851–2865, https://doi.org/10.1029/2019JG005028, 2019.

Watanabe, Y. W., Li, B. F., Yamasaki, R., Yunoki, S., Imai, K., Hosoda, S., and Nakano, Y.: Spatiotemporal changes of ocean carbon species in the western North Pacific using

parameterization technique, J. Oceanogr., 76, 155–167, https://doi.org/10.1007/s10872-019-00532-7, 2020.

Williams, N. L., Juranek, L. W., Johnson, K. S., Feely, R. A., Riser, S. C., Talley, L. D., Russell, J. L., Sarmiento, J. L., and Wanninkhof, R.: Empirical algorithms to estimate water column pH in the Southern Ocean, Geophys. Res. Lett., 43, 3415–3422, https://doi.org/10.1002/2016GL068539, 2016.

Wieners, K.-H., Giorgetta, M., Jungclaus, J., Reick, C., Esch, M., Bittner, M., Legutke, S., Schupfner, M., Wachsmann, F., Gayler, V., Haak, H., de Vrese, P., Raddatz, T., Mauritsen, T., von Storch, J.-S., Behrens, J., Brovkin, V., Claussen, M., Crueger, T., Fast, I., Fiedler, S., Hagemann, S., Hohenegger, C., Jahns, T., Kloster, S., Kinne, S., Lasslop, G., Kornblueh, L., Marotzke, J., Matei, D., Meraner, K., Mikolajewicz, U., Modali, K., Müller, W., Nabel, J., Notz, D., Peters-von Gehlen, K., Pincus, R., Pohlmann, H., Pongratz, J., Rast, S., Schmidt, H., Schnur, R., Schulzweida, U., Six, K., Stevens, B., Voigt, A. and Roeckner, E.: MPI-M MPI-ESM1.2-LR model output prepared for CMIP6 CMIP historical. doi:10.22033/ESGF/CMIP6.6595, 2019.

Wolf-Gladrow, D. A., Zeebe, R. E., Klaas, C., Körtzinger, A., and Dickson, A. G.: Total alkalinity: The explicit conservative expression and its application to biogeochemical processes, Mar. Chem., 106, 287–300, https://doi.org/10.1016/j.marchem.2007.01.006, 2007.

Wood, K. R., Bond, N. A., Danielson, S. L., Overland, J. E., Salo, S. A., Stabeno, P. J., and Whitefield, J.: A decade of environmental change in the Pacific Arctic region, Prog. Oceanogr., 136, 12–31, https://doi.org/10.1016/j.pocean.2015.05.005, 2015.

Woosley, R. J.: Evaluation of the temperature dependence of dissociation constants for the marine carbon system using pH and certified reference materials, Marine Chemistry, 229, 103914, https://doi.org/10.1016/j.marchem.2020.103914, 2021.

Woosley, R. J., Millero, F. J., and Takahashi, T.: Internal consistency of the inorganic carbon system in the Arctic Ocean, Limnol. Oceanogr. Methods, 15, 887–896, https://doi.org/10.1002/lom3.10208, 2017.

Woosley, R. J. and Millero, F. J.: Freshening of the western Arctic negates anthropogenic carbon uptake potential, Limnol. Oceanogr., 65, 1834–1846, https://doi.org/10.1002/lno.11421, 2020.

Yamamoto-Kawai, M., McLaughlin, F. A., Carmack, E. C., Nishino, S., and Shimada, K.: Aragonite undersaturation in the Arctic Ocean: effects of ocean acidification and sea ice melt, Science, 326, 1098–1100, https://doi.org/10.1126/science.1174190, 2009.

Zeng, J., Chen, M., Zheng, M., Hu, W., and Qiu, Y.: A potential nitrogen sink discovered in the oxygenated Chukchi Shelf waters of the Arctic, Geochem. Trans., 18, 5, https://doi.org/10.1186/s12932-017-0043-2, 2017.

Tables

Table 1. Chukchi Ecosystem Observatory location and instrument sampling frequency. Sensor type and parameter measured (italicized) shown in top row. Values in parenthesis indicate the number of measurements averaged over the measurement interval window.

Deployment	**Latitude**	**Longitude**	**SUNA** ***NO_3***	**HydroC CO_2** ***pCO_2***	**SBE16** ***CTD+***	**SBE37** ***CTD***	**SeaFET** ***pH***	**SBE63** ***O_2***
2016-2017	71°35'58.5600"N	161°31'06.2400"W	1 h	12 h (300/5 min)*	1 h	-	-	-
2017-2018	71°35'58.9200"N	161°31'08.0400"W	1 h	12 h (5/5 min)	2 h	2 h	2 h (30/5 min)	2 h
2018-2019	71°35'59.6400"N	161°31'41.1600"W	1 h	24 h (5/5 min)	1 h	2 h*	-	2 h*
2019-2020	71°35'58.9200"N	161°31'39.0000"W	1 h	12 h (5/5 min)	2 h	-	-	-

* indicates the sensor did not return data over the whole year due to battery failure

CTD+ indicates ancillary data was available with the SBE16 file (e.g., chlorophyll fluorescence)

Table 2. Evaluation of pH_{SeaFET} and pH^{est} using reference pH from nearby discrete samples (pH^{disc}_{calc}). Uncertainty, u_c, is the propagated combined standard uncertainty from *errors.m* (Orr et al., 2018). pH_{SeaFET} and pH^{est} were interpolated to the discrete timestamp. Figure S1 for visualization of reference values.

Date	Cruise	Cast No.	Distance (km)	$pH^{disc}_{calc} \pm u_c$	Anomaly (pH^{est}-pH^{disc}_{calc})	Anomaly (pH_{SeaFET}-pH^{disc}_{calc})	Source

2017-09-10	HLY1702	127	0.52	8.0123±0.0166	-0.0450*	-0.0354	Cross et al., 2020a
2019-08-11	HLY1901	39	3.75	7.6423±0.012	0.0079*	-	Cross et al., 2021
2019-08-19	OS1901	33	0.27	7.7367±0.0145	-0.0200	-	unpublished

* indicates pH^{disc}_{calc} was interpolated to mooring depth

1415

1416

Figures

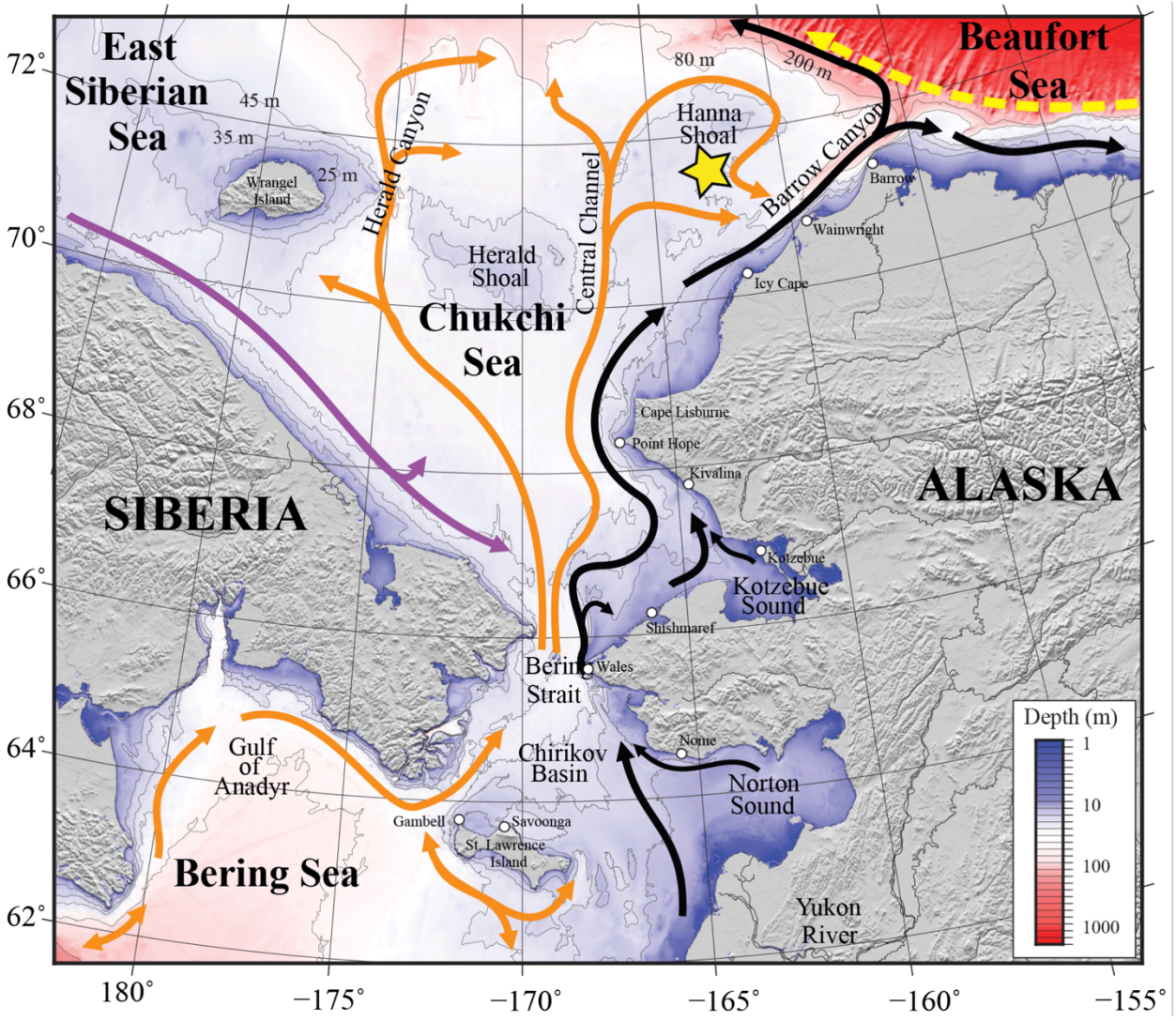

Figure 1. Map of the study area. Bathymetry of the Chukchi, northern Bering, East Siberian and eastern Beaufort seas is shown in color. The Chukchi Ecosystem Observatory (CEO) location near Hanna Shoal is marked with a yellow star. General circulation patterns are shown with arrows: black – Alaskan Coastal Water and Alaskan Coastal Current, dividing into the Shelf-break Jet (right) and Chukchi Slope Current (left, Corlett and Pickart, (2017)); orange – Anadyr, Bering, and Chukchi Seawater; purple – Siberian Coastal Current; yellow – Beaufort Gyre boundary current. Figure is from Hauri et al. (2018).

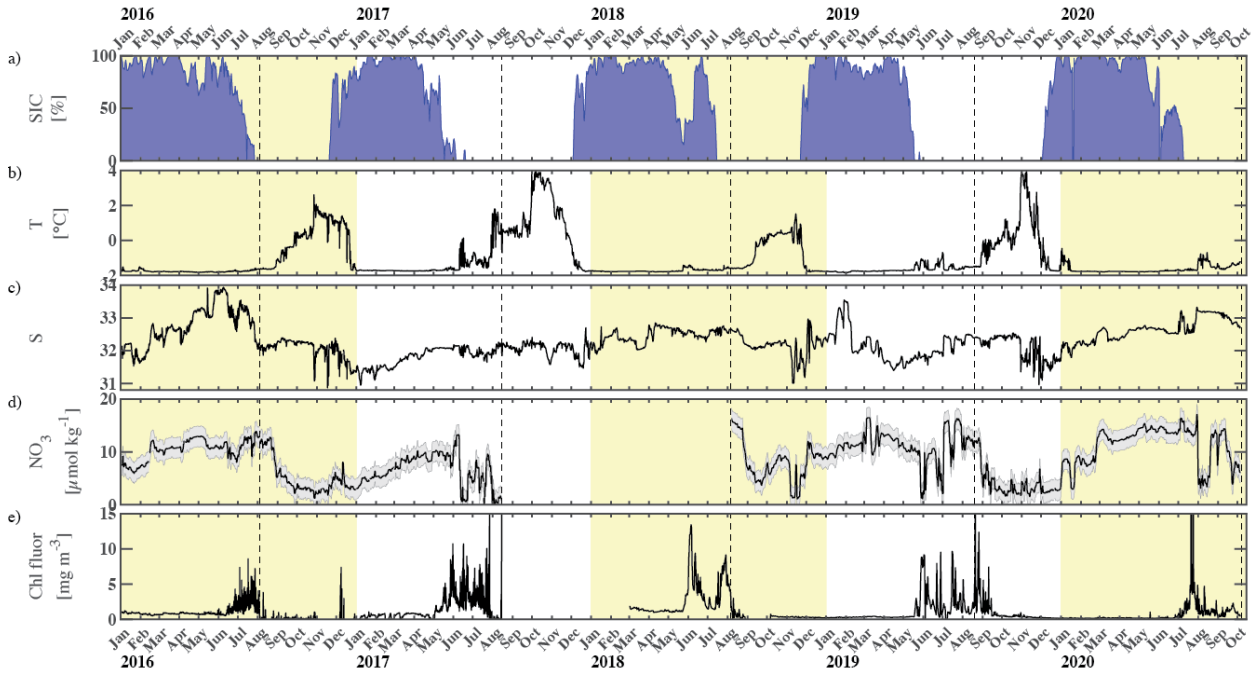

Figure 2. Chukchi Ecosystem Observatory timeseries from 2016 through 2020. a) sea ice concentration (blue shading to highlight coverage, %; DiGirolamo et al., 2022), b) temperature (°C), c) salinity, d) NO_3 with uncertainty envelope (μmol kg^{-1}), and e) chlorophyll fluorescence (mg m^{-3}). Years are indicated by alternating yellow and white background shading. The vertical dotted gray lines indicate the mooring turn around timing.

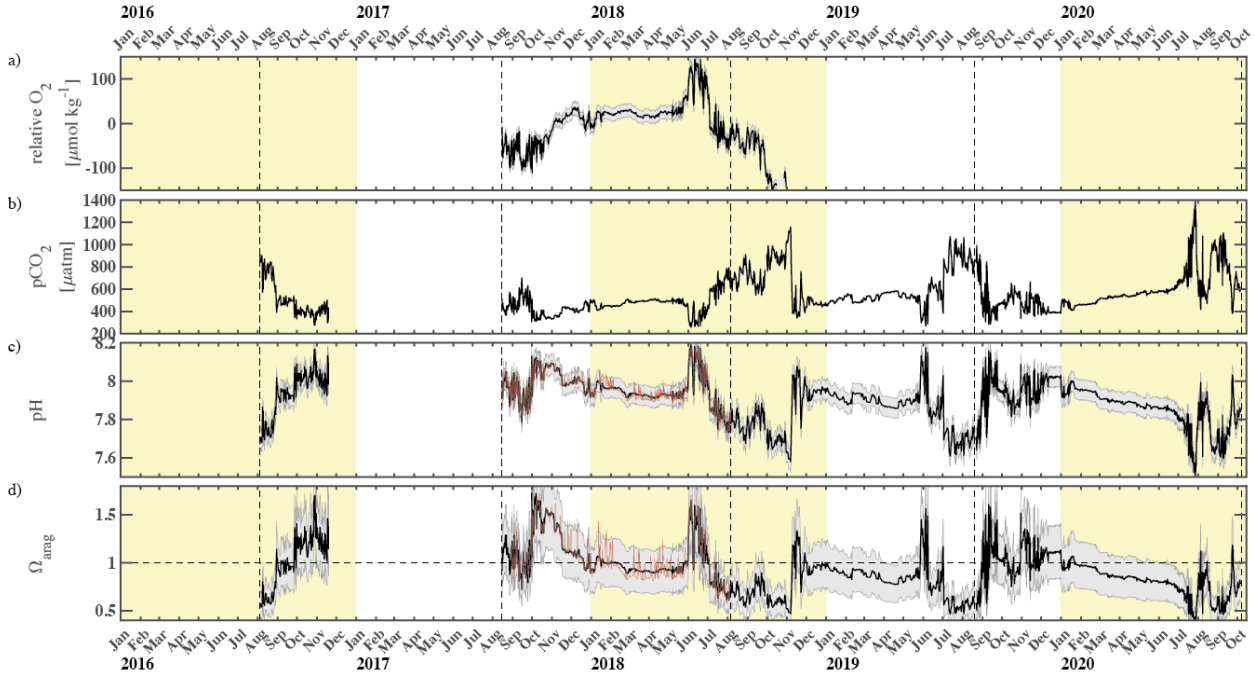

1434

1435 **Figure 3. Chukchi Ecosystem Observatory timeseries from 2016 through 2020, part 2.** a)

1436 relative dissolved oxygen with uncertainty envelope (relative to the mean; µmol kg^{-1}), b) pCO_2

1437 with uncertainty envelope (µatm; Hauri and Irving, 2023a), c) pH with uncertainty envelope

1438 (pH^{est} in black, pH_{SeaFET} in red; Hauri and Irving 2023b), and d) aragonite saturation state with

1439 uncertainty envelope ($\Omega_{arag}(pCO_2, pH^{est})$ in black; $\Omega_{arag}(pCO_2, pH_{SeaFET})$ in red). Years are

1440 indicated by alternating yellow and white backgrounds. The vertical dotted gray lines indicate

1441 the mooring turn around timing.

1442

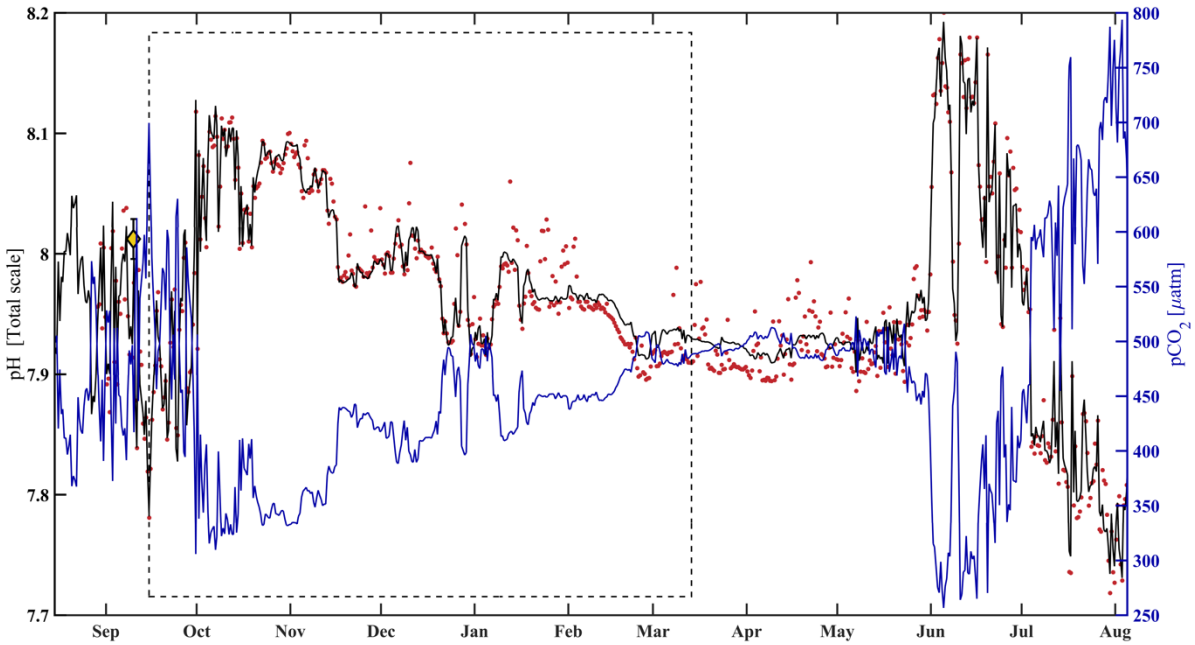

1443

1444

1445 **Figure 4. HydroC pCO_2 and pH highlighting mirrored trend from mid-August 2017 to**

1446 **beginning of August 2018.** Measured pH (pH_{SeaFET}, red dots) is interpolated onto the HydroC

1447 pCO_2 timestamp (blue), and pH^{est} is shown as the solid black line. The dashed box shows the

1448 period over which pH^{est} was trained. The yellow faced diamond with error bars show reference

1449 $pH^{disc}_{calc} \pm u_c$ (Table 2; Cross et al., 2020a; Orr et al., 2018).

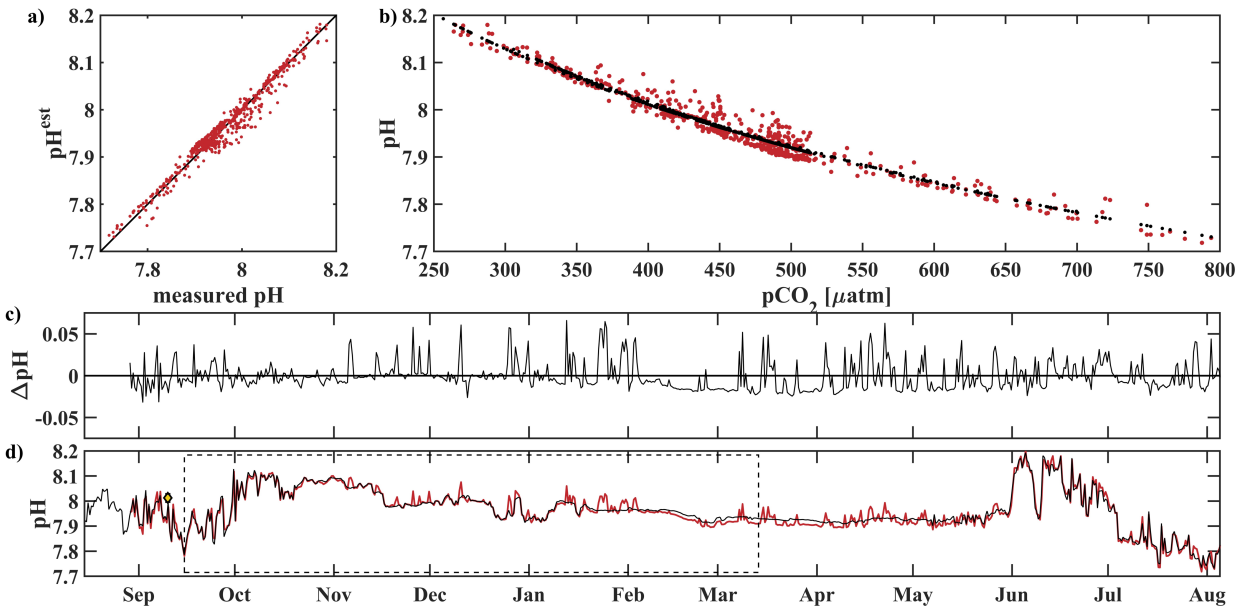

Figure 5. **Performance of the pH algorithm.** (a) pH_{SeaFET} vs pH^{est} with black line highlighting 1:1 ratio, (b) pCO_2 vs pH_{SeaFET} (red) and pCO_2 vs pH^{est} (black), (c) residual pH (pH_{SeaFET} – pH^{est}), and (d) pH_{SeaFET} (red) and pH^{est} (black) vs. time, with dashed box highlighting the period over which pH^{est} was trained (15 September - 14 March 2017), and the yellow faced diamond with error bars showing reference $pH^{disc}_{calc} \pm u_c$ (Table 2; Cross et al., 2020).

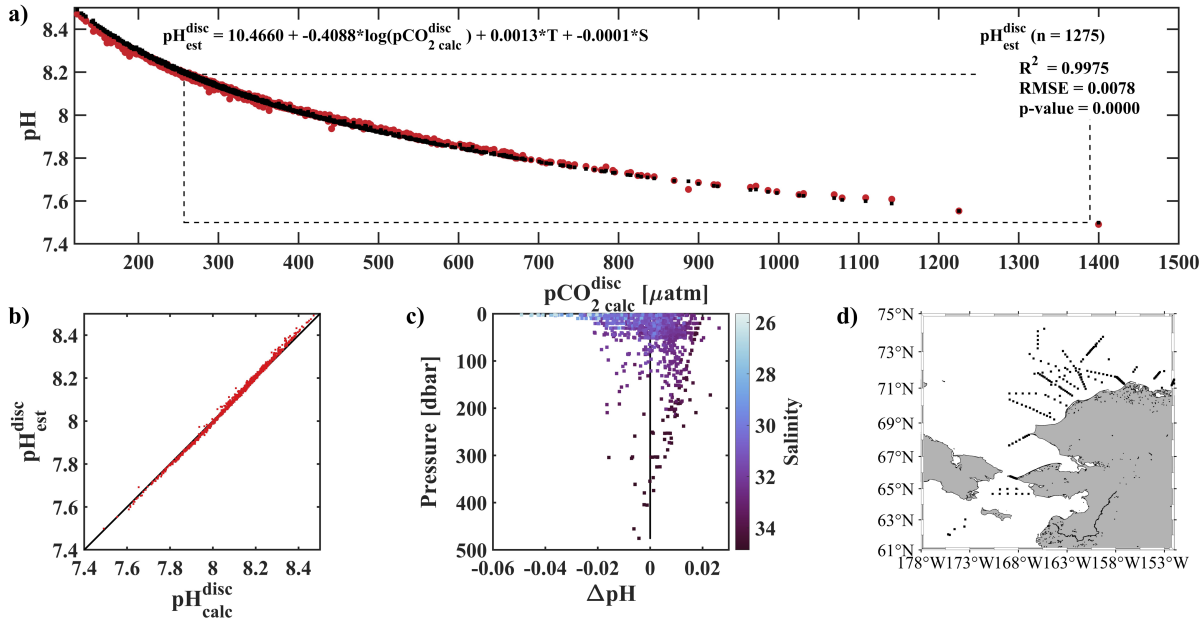

Figure 6. Evaluation of the pH algorithm. pH^{est} evaluation with pH^{disc}_{calc} from discrete samples collected during 4 cruises in the fall or early winter (August - November) of 2017-2020 and pH^{disc}_{est} from our linear regression model (Equation 2). (a) $pCO_2{}^{disc}_{calc}$(TA, DIC) vs pH (red pH^{disc}_{calc} and black pH^{disc}_{est}) with dashed black box showing the range of pH and pCO_2 observed at the CEO at 33 m depth, (b) pH^{disc}_{calc} vs pH^{disc}_{est} with black 1:1 ratio, (c) residual pH (pH^{disc}_{calc} - pH^{disc}_{est}) vs depth with color shading by salinity and black vertical line at 0, and (d) map showing the locations of the 1275 discrete water samples used for evaluation (Monacci et al., 2022; Cross et al., 2021; 2020a; 2020b).

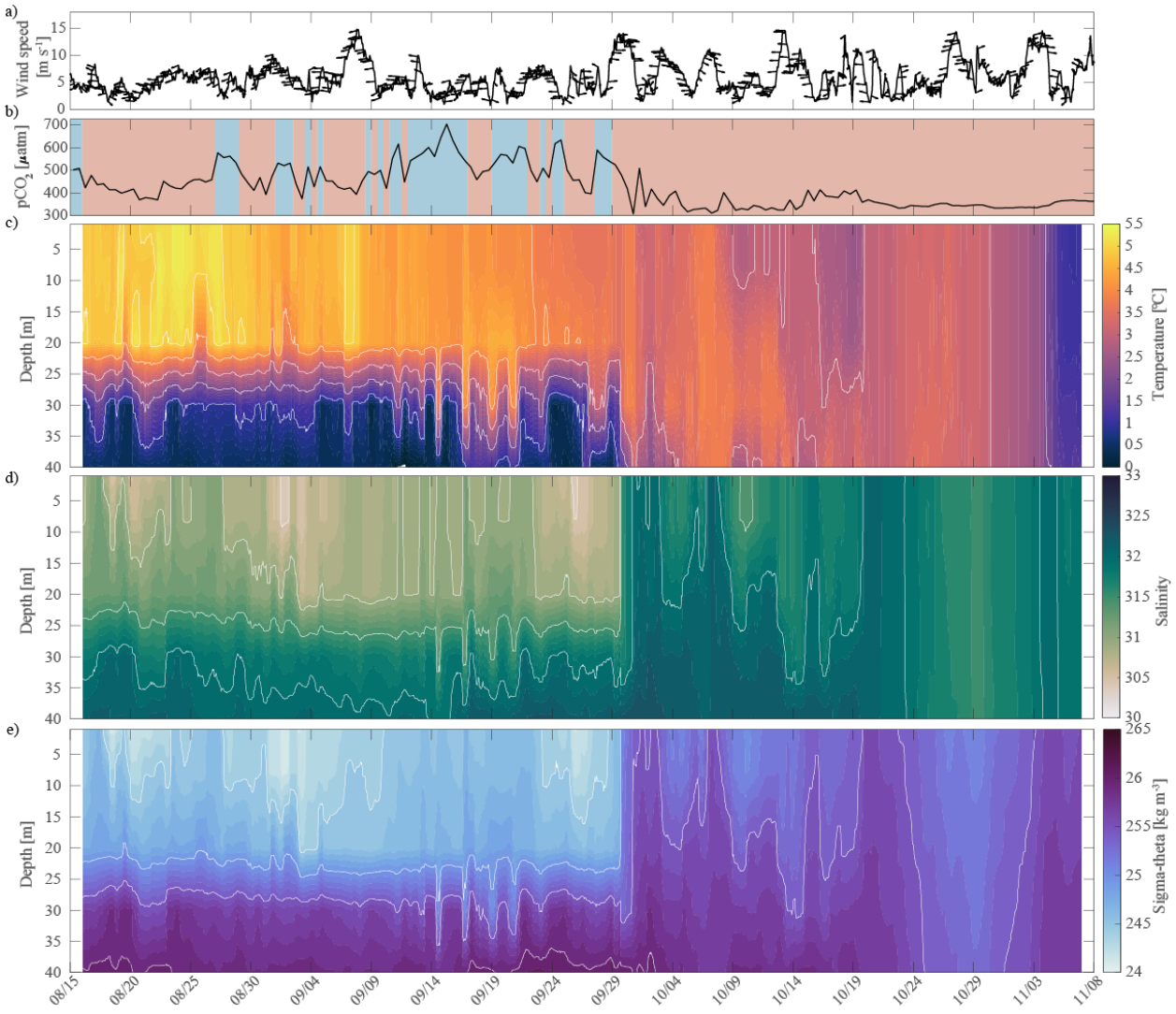

Figure 7. Water column structure from late summer 2017 to freeze up. Profiles of a) wind speed and direction (arrows pointing downwind) from the NOAA-operated Wiley Post-Will Rogers Memorial Airport, b) pCO_2 (µatm) with blue background indicating the water was undersaturated regarding aragonite ($\Omega_{arag} < 1$) and red shading indicating aragonite oversaturation ($\Omega_{arag} >= 1$), c) temperature (°C), d) salinity, and e) sigma-theta (kg m^{-3}). Temperature (c) and salinity (d) were measured at 8, 20, 30, and 40 m by the Chukchi Ecosystem Observatory freeze-up detection mooring deployed in fall 2017. Density was calculated with the TEOS-10 GSW Oceanographic Toolbox (McDougall and Baker, 2011).

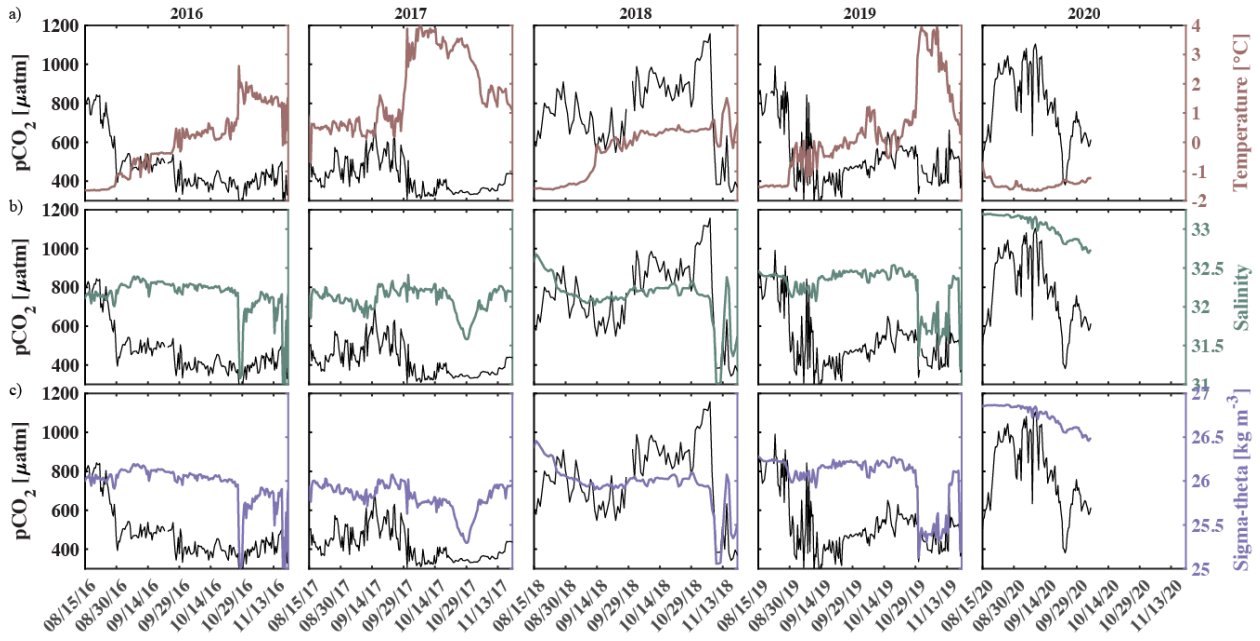

1482

1483 **Figure 8. Impact of water column mixing on pCO_2.** Timeseries of pCO_2 (black, left axis) and

1484 a) temperature (maroon, right axis), b) salinity (green, right axis), and c) density (purple, right

1485 axis) for 15 August to 1 December in 2016 -2020 measured at ~33m septh at the Chukchi Sea

1486 Ecosystem Observatory.

1487

1488

1489

1490

1491

1492

1493

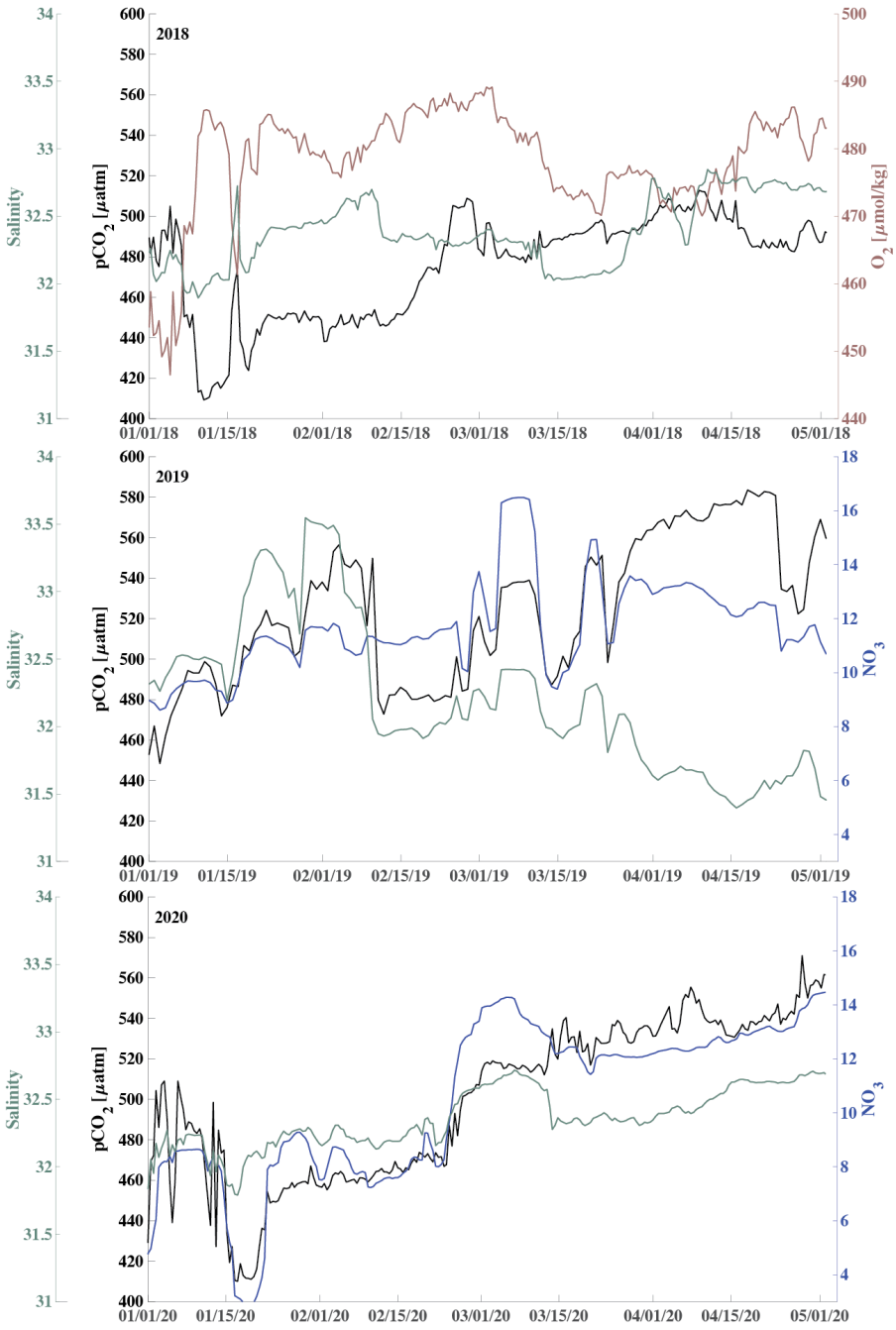

1494

1495 **Figure 9. Respiration under the sea ice.** Timeseries of pCO_2 (black) and salinity (green, left

1496 axis), and oxygen (O_2, µmol kg^{-1}, maroon, top) and nitrate (NO_3, µmol kg^{-1}, blue, middle and

1497 bottom) concentration (right axis during January through April for 2018 (top), 2019 (middle) and

1498 2020 (bottom).

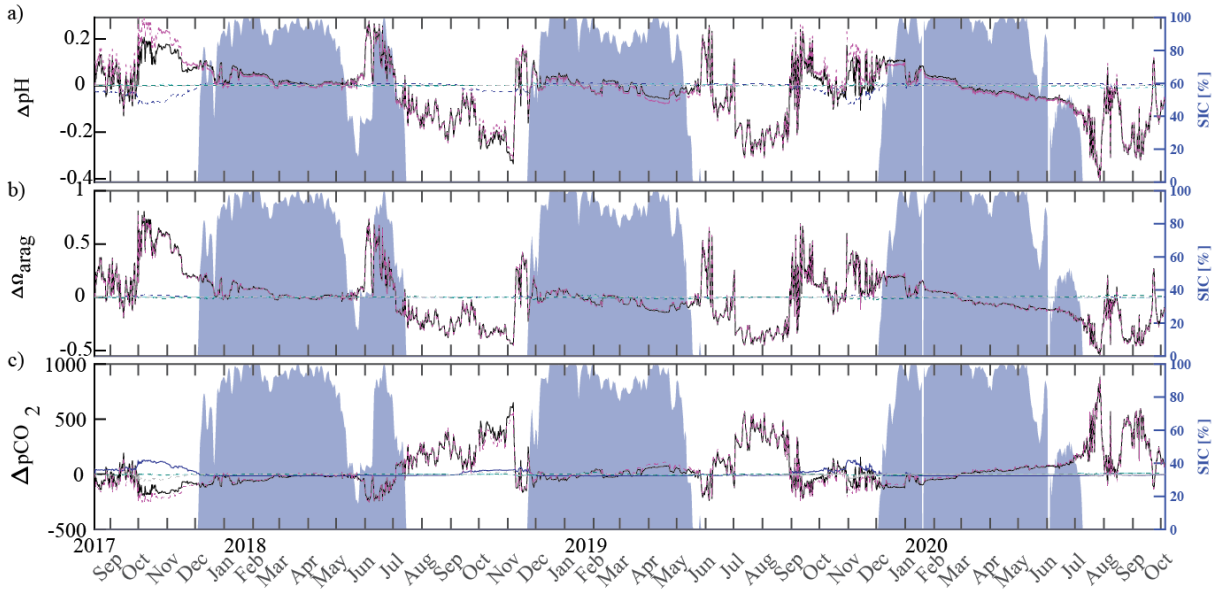

1499

1500 **Figure 10. Drivers of the inorganic carbon system.** Component timeseries of the linear Taylor
1501 decomposition of a) pH, b) Ω_{arag}, and c) pCO_2. Contributions of changes in salinity (red),
1502 temperature (blue), biogeochemistry (pink), and freshwater mixing (green) to changes (black,
1503 relative to the mean of the timeseries) in pH, Ω_{arag}, and pCO_2 were computed following Rheuban
1504 et al. (2019). The grey dotted line illustrates an estimated residual term. Sea ice concentration
1505 (blue shading, %; DiGirolamo et al., 2022) is shown on the right axes.

1506

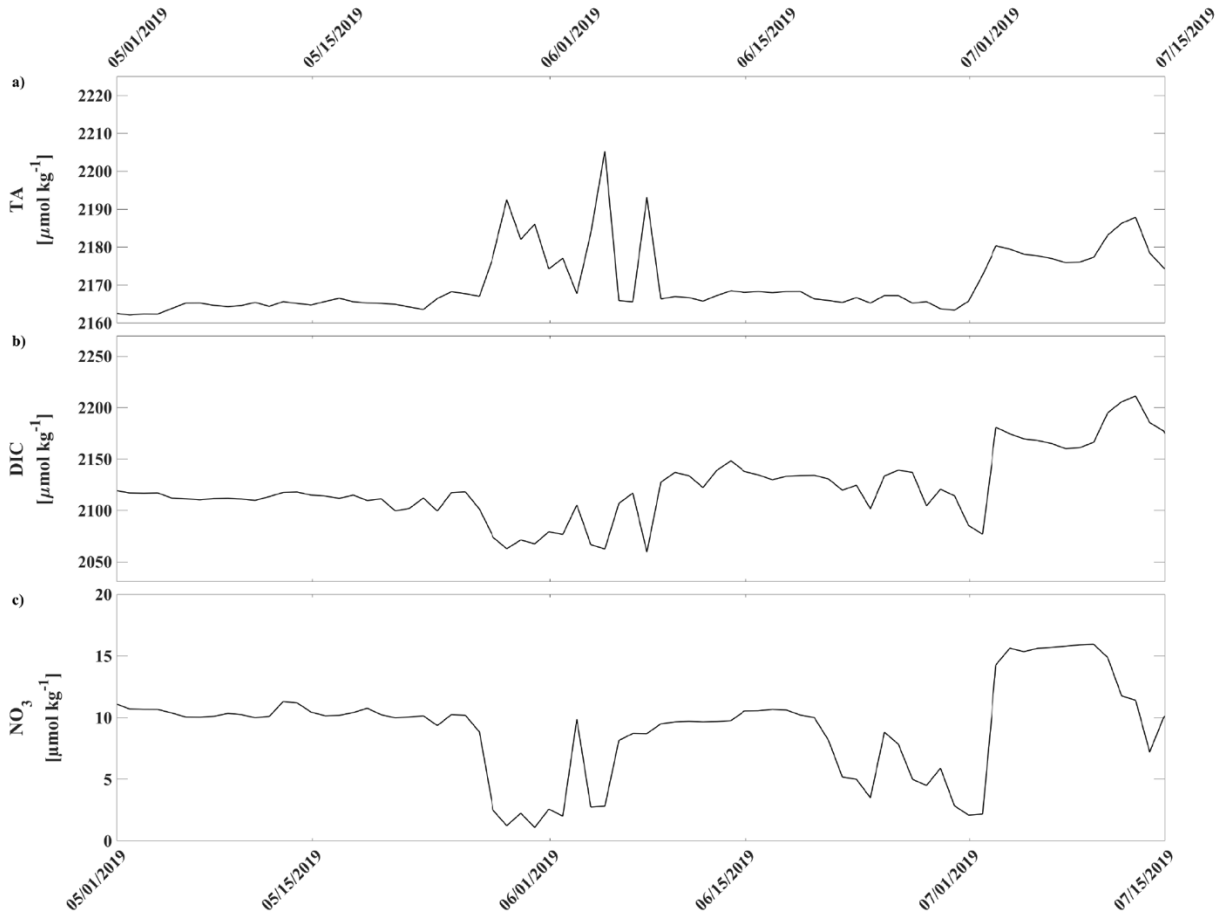

1507

1508 **Figure 11. Spring 2019 relaxation event.** Timeseries of a) total alkalinity (TA, μmol kg^{-1}), b)

1509 dissolved inorganic carbon (DIC, μmol kg^{-1}), and c) nitrate (NO_3, μmol kg^{-1}) from May 1st, 2019

1510 through July 15th, 2019.

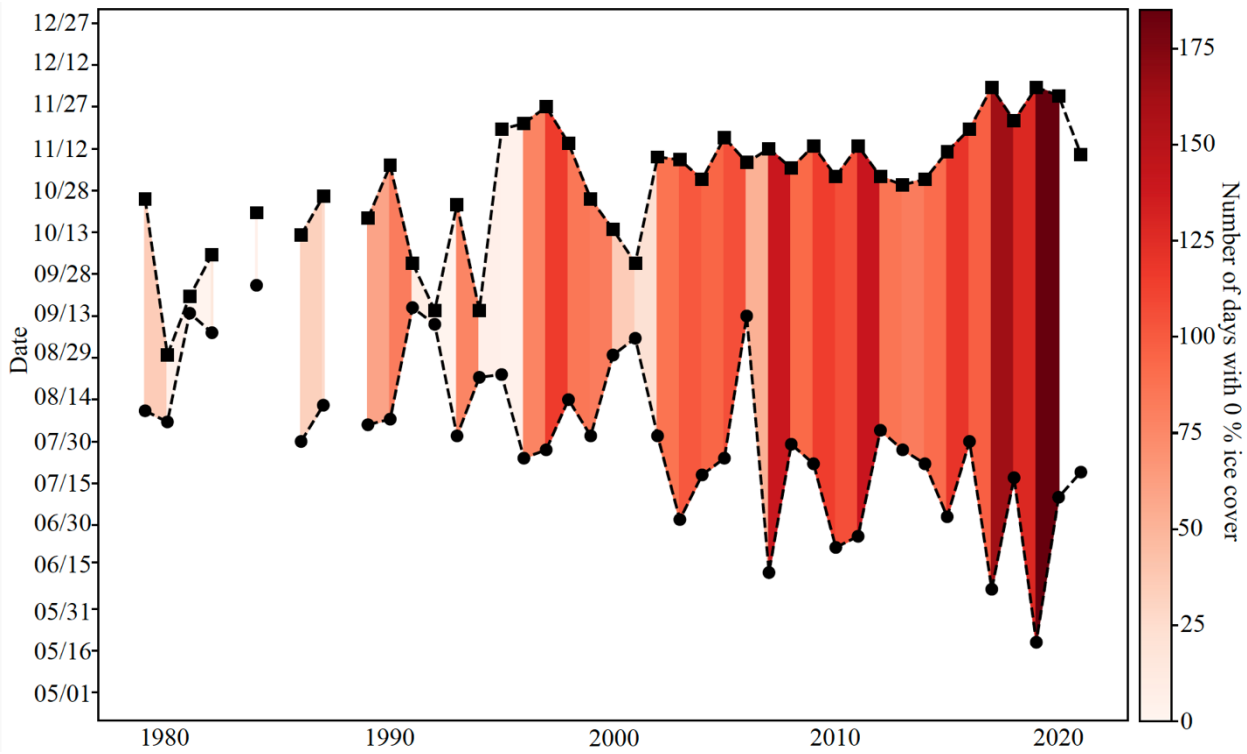

1511

1512

1513 **Figure 12. Low sea ice period at the Chukchi Sea Observatory.** Timeseries of start (circle)

1514 and end (square) of low sea ice (< 15 % per grid cell) period from 1982-2021. Shades of red

1515 illustrate number of days with 0 % sea ice cover. The satellite sea ice cover at the observatory

1516 site was taken from the NSIDC (DiGirolamo et al., 2022).

1517